

1 **Non-Hydrostatic RegCM4 (RegCM4-NH): Model description
2 and case studies over multiple domains.**

3 Coppola E. (1), Stocchi P. (2), Pichelli E. (1), Torres A. (1), Glazer R. (1), Giuliani G. (1), F. Di
4 Sante (1), R. Nogherotto (1), Giorgi F. (1)

5

6 *Correspondence to:* Erika Coppola (coppolae@ictp.it)

7 1. International Centre for Theoretical Physics (ICTP), Trieste, Italy

8 2. Institute of Atmospheric Sciences and Climate, National Research Council of Italy, CNR-ISAC,
9 Bologna, Italy

10 **Abstract**

11 We describe the development of a non-hydrostatic version of the regional climate model
12 RegCM4, called RegCM4-NH, for use at convection-permitting resolutions. The non-
13 hydrostatic dynamical core of the Mesoscale Model MM5 is introduced in the RegCM4,
14 with some modifications to increase stability and applicability of the model to long-term
15 climate simulations. Newly available explicit microphysics schemes are also described,
16 and three case studies of intense convection events are carried out in order to illustrate
17 the performance of the model. They are all run at convection-permitting grid spacing of 3
18 km over domains in northern California, Texas and the Lake Victoria region, without the
19 use of parameterized cumulus convection. A substantial improvement is found in several
20 aspects of the simulations compared to corresponding coarser resolution (12 km) runs
21 completed with the hydrostatic version of the model employing parameterized convection.
22 RegCM4-NH is currently being used in different projects for regional climate simulations
23 at convection-permitting resolutions, and is intended to be a resource for users of the
24 RegCM modeling system.

Deleted:

25

26 **Keywords:**

27 Regional climate models; RegCM4; km-scale resolution; climate change

28 **Introduction**

29 Since the pioneering work of Dickinson et al. (1989) and Giorgi and Bates (1989),
30 documenting the first regional climate modeling system (RegCM, version 1) in literature.
31 the dynamical downscaling technique based on limited area Regional Climate Models
32 (RCMs) has been widely used worldwide, and a number of RCM systems have been

34 developed (Giorgi 2019). RegCM1 (Dickinson et al., 1989, Giorgi and Bates, 1989) was
35 originally developed at the National Center for Atmospheric Research (NCAR) based on
36 the Mesoscale Model version 4 (MM4) (Anthes et al, 1987). Then, further model versions
37 followed: RegCM2 (Giorgi et al. 1993a,b), RegCM2.5, (Giorgi and Mearns 1999),
38 RegCM3 (Pal et al. 2007), and lastly RegCM4 (Giorgi et al 2012). Except for the transition,
39 from RegCM1 to RegCM2, in which the model dynamical core was updated from that of the
40 MM4 to that of the MM5 (Grell et al. 1995), these model evolutions were mostly based
41 on additions of new and more advanced physics packages. RegCM4 is today used by a
42 large community for numerous projects and applications, from process studies to paleo
43 and future climate projections, including participation in the Coordinated Regional
44 Downscaling EXperiment (CORDEX, Giorgi et al. 2009; Gutowski et al. 2016). The model
45 can also be coupled with ocean, land and chemistry/aerosol modules in a fully interactive
46 way (Sitz et al. 2017).

47 The dynamical core of the standard version of RegCM4 is hydrostatic, with sigma-p
48 vertical coordinates. As a result, the model can be effectively run for grid spacings of ~10
49 km or larger, for which the hydrostatic assumption is valid. However, the RCM community
50 is rapidly moving to higher resolutions of a few km, i.e. “convection-permitting” (Prein et
51 al. 2015; Coppola et al. 2020) and therefore the dynamical core of RegCM4 has been
52 upgraded to include a non-hydrostatic dynamics representation usable for very high
53 resolution applications. This upgrade, which we name RegCM4-NH, is essentially based
54 on the implementation of the MM5 non-hydrostatic dynamical core within the RegCM4
55 framework, which has an entirely different set of model physics compared to MM5.

56
57 RegCM4-NH is already being used in some international projects focusing on climate
58 simulations at convection-permitting km-scales, namely the European Climate Prediction
59 System (EUCP, Hewitt and Lowe 2018) and the CORDEX Flagship Pilot Study dedicated
60 to convection (CORDEX-FPSCONV, Coppola et al. 2020), and it is starting to be used
61 more broadly by the RegCM modeling community.

62 For example, the recent papers by Ban et al. (2021) and Pichelli et al. (2021) document
63 results of the first multi-model experiment of 10-year simulations at the convection-
64 permitting scales over the so-called greater Alpine region. Two different simulations with
65 RegCM4-NH for present day conditions have contributed to the evaluation analysis of
66 Ban et al. (2021). They were carried out at the International Centre for Theoretical Physics
67 (ICTP) and the Croatian Meteorological and Hydrological Service (DHMZ) using two
68 different physics configurations. The results show that RegCM4-NH largely improves the
69 precipitation simulation as compared to available fine scale observations when going from
70 coarse to high resolution, in particular for higher order statistics, such as precipitation
71 extremes and hourly intensity. Pichelli et al. (2021) then analyse multi-model ensemble
72 simulations driven by selected CMIP5 GCM projections for the decades 1996–2005 and
73 2090–2099 under the RCP8.5 scenario. ICTP contributed to the experiment with

Deleted: One of these systems, and in fact the first one to be developed, is the RegCM. The first version of RegCM, named ...egCM1 (Dickinson et al., 1989, and Bates, 1989)...was (produced by Dickinson et al., (1989), and Giorgi and Bates, (1989) as a ...riginially developeddevelopped...at the National Center for Atmospheric Research (NCAR)ment...based onf...the Mesoscale Model version 4 (MM4) (Anthes et al, 1987) of the National Center for Atmospheric Research (NCAR)... Then, is was...followed by ...urther model versions followed: RegCM2 (Giorgi et al. 1993a,b), RegCM2.5, (Giorgi and Mearns 1999), RegCM3 (Pal et al. 2007), and lastly

... [1]

Deleted: passage...from RegCM1 to RegCM2, in which the model dynamical core was updated from that of the MM4 to that of the MM5 (Grell et al. 1995), these model evolutions were mostly based on additions of new and more advanced sub-grid..physics packages. In particular, ...egCM4 is today used by a large community for numerous projects and applications, from process studies to paleo and future climate projections, including participation into

... [2]

Deleted: more

Deleted: Long term simulations carried out through the new generation ...egCM4-NH is already being used incontribute to...some internationalbroad..projects focusing ondedicated to the study of...climate at the...convection-permitting km-scales,...namely the European Climate Prediction System (EUCP, Hewitt and Lowe 2018) and the CORDEX Flagship Pilot Study dedicated to convection (CORDEX-FPSCONV, Coppola et al. 2020), and it is starting to be used more broadly by the RegCM modeling community. ¶

... [3]

Deleted: T...he recent papers by Ban et al. (2021) and Pichelli et al. (2021) document results of the first multi-model experiment of 10-year simulations at the convection-permitting scales over the so-called greater Aa...pine region. Two different simulations with RegCM4-NH for over the...present day conditions...have contributed to the evaluation analysis offor precipitation...(...an et al....(2021). They...wererespectively...carried out atby the research group of...the International Centre for Theoretical Physics (ICTP) and the Croatian Meteorological and Hydrological Service (DHMZ) usingwith...two different physiscal... ¶

... [4]

Deleted: EG

Deleted: simulations...largely improves reduce...the precipitation simulation asbiasas

... [5]

Deleted: with...available fine scale observations when going from coarse to higher

... [6]

Deleted: contributing to adding value to the representation of rainfall... Pichelli et al. (2021) then analyserepresent the...multi-model ensemble simulations driven by selected CMIP5 GCM projections for theover... ¶

Deleted: rcp

180 simulations using RegCM4-NH driven by the MOCH-HadGEM GCM (r1i1p1) in a two
181 level nest configuration (respectively at 12 and 3 km grid). The paper shows new insights
182 into future changes, for example an enhancement of summer and autumn hourly rainfall
183 intensification compared to coarser resolution model experiments, as well as an increase
184 of frequency and intensity of high-impact weather events.

Deleted: performed by the new
Deleted: core
Deleted: with, among the others,
Deleted: more than previously documented by
Deleted: frequency

185
186 In this paper we describe the structure of RegCM4-NH and provide some illustrative
187 examples of its performance, so that model users can have a basic reference providing
188 them with background information on the model. In the next section we first describe the
189 new model dynamical core, while the illustrative applications are presented in section 4.
190 Section 5 finally provides some discussion of future developments planned for the RegCM
191 system.
192

193 **Model description**

194 In the development of RegCM4-NH, the RegCM4 as described by Giorgi et al. (2012) was
195 modified to include the non-hydrostatic dynamical core (*idynamic* = 2 namelist option as
196 described in RegCM-4.7.1/Doc/README.namelist of the source code) of the mesoscale
197 model MM5 (Grell et al. 1995). This dynamical core was selected because RegCM4
198 already has the same grid and variable structure as MM5 in its hydrostatic core, which
199 substantially facilitated its implementation (Elguindi et al. 2017).

Deleted: as an additional option selectable through a
switch,...
Deleted: . which uses the equations described by Grell
et al. (1995)...
Deleted: shares with it
Deleted: it
Deleted: follows
Deleted: for
Deleted: of the RegCM4
Deleted: standard

200
201 The model equations with complete description of the Coriolis force and a top radiative
202 boundary condition, along with the finite differencing scheme, are given in Grell et al.
203 (1995). Pressure, p , temperature, T , and density, ρ , are first decomposed into a
204 prescribed reference vertical profile plus a time varying perturbation. The prognostic
205 equations are then calculated using the pressure perturbation values. Compared to the
206 original MM5 dynamical core, the following modifications were implemented in order to
207 achieve increased stability for long term climate simulations (Elguindi et al. 2017)
208 document any modifications which follow the choice of the non-hydrostatic dynamical
209 core through the namelist parameter *idynamic* = 2; further available user-dependant
210 options, and the corresponding section in the namelist, are explicitly indicated):
211

212 i) The reference state temperature profile is computed using a latitude dependent
213 climatological temperature distribution and thus is a function of the specific domain
214 coordinates (*base_state_pressure*, *logp_lrate* parameters in *&referenceatm*) (Elguindi et
215 al. 2017). These two parameters were hard-coded in the original MM5 while for the
216 RegCM are user configurable;

Deleted: surface

Commented [1]: added the configurability comment
here-

234 ii) The lateral time dependent boundary conditions (*iboudy* in *&physicsparam*) for each
235 prognostic variable use the same exponential relaxation technique (*iboudy* = 5) described
236 in Giorgi et al. (1993). The linear MM5 relaxation scheme is also kept as an option (*iboudy*
237 = 1);

Deleted: only

238
239 iii) The advection term in the model equations, which in the MM5 code is implemented
240 using a centered finite difference approach, was changed to include a greater upstream
241 weight factor as a function of the local Courant number (Elguindi et al. 2017). The
242 maximum value of the weight factor is user configurable (*uoffc* in *&dynparam*). As detailed
243 in the MM5 model description (Grell et al, 1995), the horizontal advection term for a scalar
244 variable *X* contributes to the total tendency as:

$$\Delta_{adv} (p^* X)_G = -m^2|_G \left[\frac{(p^* X|_b \frac{u}{m}|_b - p^* X|_a \frac{u}{m}|_a)}{dx} + \frac{(p^* X|_d \frac{v}{m}|_d - p^* X|_c \frac{v}{m}|_c)}{dy} \right]$$

245
246 where the *m* is the projection mapping factor and, with respect to Figure 1, assuming that
247 the computation is to be performed for the gold cross point *G*, the averages are performed
248 in the points *a, b, c, d*. For the *u/m* and *v/m* terms, the average value is computed using
249 respectively the values in points *AC, BD, CD, AB*.

Commented [2]: Added the equation description-

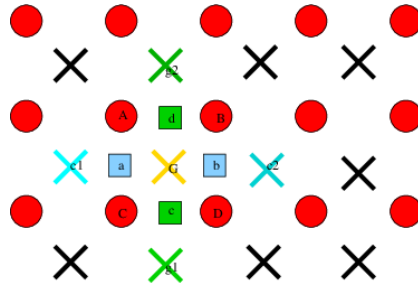
250 In RegCM4 for the term *p^{*}X*, the model computes a weighted average value of the field
251 using the value in gold+cyan and gold+green cross points with weights increasing the
252 relative contribution of the upstream point up as a function of the local courant number:

$$\begin{aligned} p^* X|_a &= 0.5((1 - f_1)p^* X|_G + (1 + f_1)p^* X|_{c_1}) \\ p^* X|_b &= 0.5((1 - f_1)p^* X|_{c_2} + (1 + f_1)p^* X|_G) \\ p^* X|_c &= 0.5((1 - f_2)p^* X|_G + (1 + f_2)p^* X|_{g_1}) \\ p^* X|_d &= 0.5((1 - f_2)p^* X|_{g_2} + (1 + f_2)p^* X|_G) \end{aligned}$$

253 where *f₁, f₂* are defined as the local Courant number for the 1D advection equations
254 multiplied for a control factor:

$$\begin{aligned} f_1 &= \mu_{fc} dt \frac{(u|_a + u|_b)}{2dx} \\ f_2 &= \mu_{fc} dt \frac{(v|_c + v|_d)}{2dy} \end{aligned}$$

Commented [3]: Added equation description



267
268 Figure 1 Schematic representation showing the horizontal advection scheme
269 staggering. Circles are U,V points. X are scalar variable points.

270
271
272
273 iv) The water species (cloud, ice, rain, snow) term uses the same advection scheme as
274 the other variables (Elguindi et al. 2017) and not a complete upstream scheme as in the
275 MM5 code (Grell et al. 1995);

Deleted: moisture

276
277 v) A local flux limiter reduces the advection terms in order to remove unrealistic strong
278 gradients and its limits are user configurable (in the &dynparam section the maximum
279 gradient fraction for advection; temperature, t_extrema, specific humidity, q_rel_extrema,
280 liquid cloud content, c_rel_extrema and for tracers, t_rel_extrema). This was hardcoded
281 in the MM5 code and the limits were not user configurable;

Deleted: to stop for

282
283 vi) The diffusion stencil of the Laplace equation uses a nine point approach as in LeVeque
284 (2006) and a topography dependent environmental diffusion coefficient is added to
285 reduce spurious diffusion along pressure coordinate slopes (Elguindi et al. 2017) as in
286 the hydrostatic version of the code (Giorgi et al. 1993b). The change in stencil does not
287 affect the overall fourth order precision of the model, but reduces the computational
288 stencil size, thus reducing the communication overhead;

Deleted: used

289
290 vii) The top boundary radiative condition (ifupr = 1 in &nonhydroparam) adopted in the
291 semi-implicit vertical differencing scheme to reduce the reflection of energy waves uses
292 coefficients on a 13x13 matrix which are re-computed every simulation day and not kept
293 constant throughout the whole simulation as in the MM5 code. This allows the model to
294 be run for longer simulation times while not being strongly tied to the initial atmospheric
295 conditions;

296

300 viii) The dynamical control parameter β in the semi-implicit vertical differencing scheme
 301 (*nhbet* in *&nonhydromodel*) used for acoustic wave damping (Elguindi et al. 2017) is user
 302 configurable (Klemp and Dudhia, 2008), while it is hard-coded in the MM5;

Deleted: is
 Deleted: and
 Deleted: code

303
 304 ix) A Rayleigh damping (*ifrayd* = 1 in *&nonhydromodel*) of the status variables towards
 305 the input GCM boundary conditions can be activated in the top layers (*rayndamp*
 306 configuring the number of top levels to apply) with a configurable relaxation time
 307 (*rayalpha0*, Klemp and Lilly, 1978, Durran and Klemp, 1983. This is consistent to what is
 308 implemented in the WRF model);

309
 310 x) The water species time filtering uses the Williams (2009) modified filter with $\alpha = 0.53$
 311 instead of the RA filter used by all the other variables. The v factor in the RA filter is user
 312 configurable (*gnu1* and *gnu2* in *&dynparam*). This reduces the damping introduced by the
 313 Robert-Asselin filter and the computational diffusion introduced by the horizontal
 314 advection scheme.

Deleted: the (same as in the MM5) and namely
 Deleted: are

315
 316 With these modifications, the model basic equations, under leap-frog integration scheme,
 317 are, (Elguindi et al. 2017) :

$$\frac{\partial p^* u}{\partial t} = -m^2 \left[\frac{\partial p^* uu/m}{\partial x} + \frac{\partial p^* vu/m}{\partial y} \right] - \frac{\partial p^* u \dot{\sigma}}{\partial \sigma} + u DIV - \frac{mp^*}{\rho} \left[\frac{\partial p'}{\partial x} - \frac{\sigma}{p^*} \frac{\partial p^*}{\partial x} \frac{\partial p'}{\partial \sigma} \right] + p^* fv - p^* ew \cos \theta + D_u \quad (1)$$

$$\frac{\partial p^* v}{\partial t} = -m^2 \left[\frac{\partial p^* uv/m}{\partial x} + \frac{\partial p^* vv/m}{\partial y} \right] - \frac{\partial p^* v \dot{\sigma}}{\partial \sigma} + v DIV - \frac{mp^*}{\rho} \left[\frac{\partial p'}{\partial y} - \frac{\sigma}{p^*} \frac{\partial p^*}{\partial y} \frac{\partial p'}{\partial \sigma} \right] - p^* fu + p^* ew \sin \theta + D_v \quad (2)$$

$$\frac{\partial p^* w}{\partial t} = -m^2 \left[\frac{\partial p^* uw/m}{\partial x} + \frac{\partial p^* vw/m}{\partial y} \right] - \frac{\partial p^* w \dot{\sigma}}{\partial \sigma} + w DIV + p^* g \frac{\rho_0}{\rho} \left[\frac{1}{p^*} \frac{\partial p'}{\partial \sigma} + \frac{T_v'}{T} - \frac{T_0 p'}{T_0 p_0} \right] - p^* g [(q_e + q_r)] + p^* e (u \cos \theta - v \sin \theta) + D_w \quad (3)$$

$$\frac{\partial p^* p'}{\partial t} = -m^2 \left[\frac{\partial p^* up'/m}{\partial x} + \frac{\partial p^* vp'/m}{\partial y} \right] - \frac{\partial p^* p' \dot{\sigma}}{\partial \sigma} + p' DIV - m^2 p^* \gamma p \left[\frac{\partial u/m}{\partial x} - \frac{\sigma}{mp^*} \frac{\partial p^*}{\partial x} \frac{\partial u}{\partial \sigma} + \frac{\partial v/m}{\partial y} - \frac{\sigma}{mp^*} \frac{\partial p^*}{\partial y} \frac{\partial v}{\partial \sigma} \right] + \rho_0 g \gamma p \frac{\partial w}{\partial \sigma} + p^* \rho_0 g \quad (4)$$

332

$$\frac{\partial p^* T}{\partial t} = -m^2 \left[\frac{\partial p^* u T / m}{\partial x} + \frac{\partial p^* v T / m}{\partial y} \right] - \frac{\partial p^* T \dot{\sigma}}{\partial \sigma} + T DIV +$$

$$\frac{1}{\rho c_p} \left[p^* \frac{D p'}{D t} - \rho_0 g p^* w - D_{p'} \right] + p^* \frac{\dot{Q}}{c_p} + D_T \quad (5)$$

333

334

335 Where:

$$DIV = m^2 \left[\frac{\partial p^* u / m}{\partial x} + \frac{\partial p^* v / m}{\partial y} \right] + \frac{\partial p^* \dot{\sigma}}{\partial \sigma}$$

$$\dot{\sigma} = -\frac{\rho_0 g}{p^*} w - \frac{m \sigma}{p^*} \frac{\partial p^*}{\partial x} u - \frac{m \sigma}{p^*} \frac{\partial p^*}{\partial y} v$$

$$\tan \theta = -\cos \phi \frac{\partial \lambda / \partial y}{\partial \phi / \partial x}$$

$$p(x, y, z, t) = p_0(z) + p'(x, y, z, t)$$

$$T(x, y, z, t) = T_0(z) + T'(x, y, z, t)$$

$$\rho(x, y, z, t) = \rho_0(z) + \rho'(x, y, z, t)$$

340

341 with the vertical sigma coordinate defined as:

342

$$\sigma = \frac{(p_0 - p_t)}{(p_s - p_t)}$$

343

344 where p_s is the surface pressure and p_0 is the reference pressure profile. The total
345 pressure

346 at each grid point is thus given as:

347

$$p(x, y, z, t) = p^* \sigma(k) + p_t + p'(x, y, z, t)$$

348

349 With p_t being the top model pressure assuming a fixed rigid lid.

350

351

Deleted: and

Deleted: is

354 The model physics schemes for boundary layer, radiative transfer, land and ocean
 355 surface processes, cloud and precipitation processes are extensively described in Giorgi
 356 et al. (2012) and summarized in Table 1. For each physics component a number of
 357 parameterization options are available (Table 1), and can be selected using a switch
 358 selected by the user. As mentioned, the use of non-hydrostatic dynamics is especially
 359 important when going to convection-permitting resolutions of a few km (Prein et al. 2015).
 360 At these resolutions the scale separation assumption underlying the use of cumulus
 361 convection schemes is not valid any more, and explicit cloud microphysics
 362 representations are necessary. The RegCM4 currently includes two newly implemented
 363 microphysics schemes, the Nogherotto-Tompkins (Nogherotto et al. 2016) and the WSM5
 364 scheme from the Weather Research Forecast (WRF, Skamarok et al. 2008) model, which
 365 are briefly described in the next sections for information to model users.

Deleted: resumed

Deleted: references therein

Deleted: model

<u>Model physics</u> <u>(Namelist flag)</u>	<u>Options</u>	<u>n. option</u>	<u>Reference</u>
<u>Dynamical core</u> <u>(idynamic)</u>	Hydrostatic	<u>1</u>	<u>Giorgi et al. 1993a,b</u> <u>Giorgi et al. 2012</u>
	Non-Hydrostatic (*)	<u>2</u>	<u>present paper</u>
<u>Radiation</u> <u>(irrtm)</u>	CCSM	<u>0</u>	<u>Kiehl et al. 1996</u>
	RRTM (*)	<u>1</u>	<u>Mlawer et al. 1997</u>
<u>Microphysics</u> <u>(ipptls)</u>	Subex	<u>1</u>	<u>Pal et al 2000</u>
	Nogherotto Tompkins	<u>2</u>	<u>Nogherotto et al. 2016</u>
	WSM5 (*)	<u>3</u>	<u>Hong et al 2004</u>
<u>Cumulus</u> <u>(icup)</u>	Kuo	<u>1</u>	<u>Anthes et al. 1987</u>
	Grell	<u>2</u>	<u>Grell 1993</u>
	Emanuel	<u>4</u>	<u>Emanuel 1991</u>
	Tiedtke	<u>5</u>	<u>Tiedtke 1989, 1993</u>

	Kain-Fritsch	<u>6</u>	Kain and Fritsch, 1990; Kain 2004
	MM5 Shallow cumulus (only mixing) (*)	<u>-1</u>	Grell et al. 1994
<u>Planetary Boundary Layer</u> <u>(ibltyp)</u>	Modified-Holtslag	<u>1</u>	Holtslag et al., 1990
	<u>UW</u>	<u>2</u>	Bretherton et al. 2004
<u>Land Surface</u> <u>(code compiling option)</u>	BATS	<u>1</u>	Dickinson et al. 1993; Giorgi et al. 2003
	CLM4.5	<u>1</u>	Oleson et al. 2013
<u>Ocean Fluxes</u> <u>(iocnflux)</u>	BATS	<u>1</u>	Dickinson et al. 1993
	Zeng	<u>2</u>	Zeng et al. 1998
	COARE	<u>3</u>	Fairall et al. 1996a,b
<u>Interactive lake</u> <u>(lakemod)</u>	1D diffusion/convection	<u>1</u>	Hostetler et al. 1993
<u>Tropical band</u> <u>(i_band)</u>	RegT-Band	<u>1</u>	Coppola et al. 2012
<u>Coupled ocean</u> <u>(iocncpl)</u>	RegCM-ES	<u>1</u>	Sitz et al. 2017

370 **Table 1 Core and sub-grid physics scheme available in RegCM-NH. New schemes**
 371 **available with this release are starred (*).**

372
 373
 374 **Explicit microphysics schemes:**

375

Formatted: Font: 12 pt, Font colour: Auto
 Formatted: Normal

376 *Nogherotto-Tompkins Scheme:*

377 A new parameterization for explicit cloud microphysics and precipitation built upon the
378 European Centre for Medium Weather Forecast's Integrated Forecast System (IFS)
379 module (Tiedtke, 1993, Tompkins, 2007), was introduced in RegCM4 (*ipptls* = 2 in
380 *µparam*) by Nogherotto et al. (2016). In the present configuration, the scheme
381 implicitly solves 5 prognostic equations for water vapor, qv, cloud liquid water, ql, rain, qr,
382 cloud ice, qi, and snow, qs, but it is also easily extendable to a larger number of variables.
383 Water vapor, cloud liquid water, rain, cloud ice and snow, are all expressed in terms of the
384 grid-mean mixing ratio.

Deleted: solves implicitly

Deleted: qv

Deleted: ql

Deleted: qr

Deleted: qi

Deleted: qs

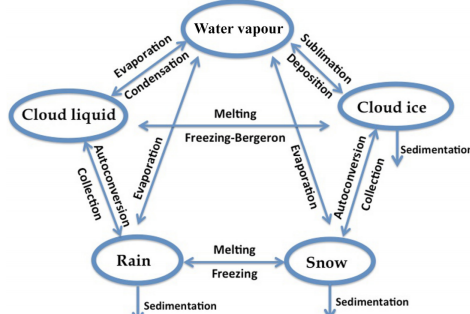
385 Cloud liquid and ice water content are independent, allowing the existence of supercooled
386 liquid water and mixed-phase clouds. Rain and snow precipitate with a fixed terminal fall
387 speed and can then be advected by the three dimensional winds. A check for the
388 conservation of enthalpy and of total moisture is ensured at the end of each timestep. The
389 governing equation for each variable is:
390

$$\frac{\partial q_x}{\partial t} = S_x + \frac{1}{\rho} \frac{\partial}{\partial z} (\rho V_x q_x)$$

391
392
393 The local variation of the mixing ratio q_x of the variable x is given by the sum of S_x ,
394 containing the net sources and sinks of q_x through microphysical processes (i.e.
395 condensation, evaporation, auto-conversion, melting, etc.), and the sedimentation term,
396 which is a function of the fall speed V_x . An upstream approach is employed to solve the
397 equations. The sources and sinks contributors are divided in two groups according to the
398 duration of the process they describe: processes that are considered to be fast relative to
399 the model time step are treated implicitly while slow processes are treated explicitly. The
400 processes taken into account (shown in Figure 2) are the microphysical pathways across
401 the 5 water variables: condensation, autoconversion, evaporation, cloud water collection
402 (accretion), and autoconversion for warm clouds, and freezing, melting, deposition,
403 sublimation for cold clouds.

Deleted: 1

404



412

413 **Figure 2: Depiction of the new scheme, showing the five prognostic variables and**
 414 **how they are related to each other through microphysical processes**

Deleted: 1

415 For each microphysical pathway, phase changes are associated with the release or
 416 absorption of latent heat, which then impacts the temperature budget. The impact is
 417 calculated using the conservation of liquid water temperature T_L defined as:

418

419

$$T_L = T - \frac{L_v}{C_p} (q_l + q_r) - \frac{L_s}{C_p} (q_i + q_s).$$

420 Given that $dT_L = 0$, the rate of change of the temperature is given by the following
 421 equation:

422

423

$$\frac{\partial T}{\partial t} = \sum_{x=1}^m \frac{L(x)}{C_p} \left(\frac{dq_x}{dt} - D_{q_x} - \frac{1}{\rho} \frac{\partial}{\partial z} (\rho V_x q_x) \right)$$

424

425 where $L(x)$ is the latent heat of fusion or evaporation, depending on the process
 426 considered, D_{q_x} is the convective detrainment and the third term in brackets is the
 427 sedimentation term.

428 At the end of each time step a check is carried out of the conservation of total water and
 429 moist static energy:

$$h = C_p T + gz + L q_x.$$

430 The scheme is tunable through parameters in the `µparam` section of the namelist
 431 (RegCM-4.7.1/Doc/README.namelist; Elguindi et al. 2017).

433 WSM5 Scheme:

434 RegCM4-NH also employs the Single-Moment 5-class microphysics scheme of the WRF
435 model (Skamarock et al., 2008). This scheme (*ipptls* = 3 in *µparam*) follows Hong
436 et al. (2004) and, similarly to Nogherotto et al. (2016), includes vapor, rain, snow, cloud
437 ice, and cloud water hydrometeors. The scheme separately treats ice and water
438 saturation processes, assuming water hydrometeors for temperatures above freezing,
439 and cloud ice and snow below the freezing level (Dudhia, 1989, Hong et al., 1998). It
440 accounts for supercooled water and a gradual melting of snow below the melting layer
441 (Hong et al., 2004, and Hong and Lim, 2006). Therefore, the WSM5 and Nogherotto-
442 Tompkins schemes have similar structures (Figure 2), but also important differences.

Deleted: 1

443 Differently from the Nogherotto-Tompkins scheme, the WSM5 (as well as the other WSM
444 schemes in WRF) prescribes an inverse exponential continuous distribution of particle
445 size (ex. Marshall and Palmer (1948) for rain, Gunn and Marshall (1958) for snow). It also
446 includes the size distribution of ice particles and, as a major novelty, the definition of the
447 number of ice crystals based on ice mass content rather than temperature. Both the
448 Nogherotto-Tompkins and WSM5 schemes include autoconversion, i.e. sub-time step
449 processes of conversion of cloud water to rain and cloud ice to snow. For rain, Hong et
450 al. (2004) use a Kessler (1969) type algorithm in WSM5, but with a stronger physical basis
451 following Tripoli and Cotton (1980). The Nogherotto-Tompkins scheme also includes the
452 original Kessler (1969) formula as an option, but it makes available other three
453 exponential approaches following Sundqvist et al. (1989), Beheng (1994), and
454 Khairoutdinov and Kogan (2000). For ice autoconversion the Nogherotto-Tompkins
455 scheme uses an exponential approach (Sundqvist, 1989) with a specific coefficient for ice
456 particles (following Lin et al., 1983) depending on temperature, while the WSM5 uses a
457 critical value of ice mixing ratio (depending on air density) and a maximum allowed ice
458 crystal mass (following Rutledge and Hobbs, 1983) that suppresses the process at low
459 temperatures because of the effect of air density. Finally, the WSM5 has no dependency
460 on cloud cover for condensation processes while the Nogherotto-Tompkins scheme uses
461 cloud cover to regulate the condensation rate in the formation of stratiform clouds.

462

463 **Illustrative case studies**

464
465 Three case studies (Table 2) of Heavy Precipitation Events (HPE) have been identified in
466 order to test and illustrate the behavior of the non-hydrostatic core of the RegCM4-NH,
467 with focus on the explicit simulation of convection over different regions of the world. In
468 two test cases, California and Lake Victoria, data from the ERA-Interim reanalysis (Dee

Deleted: 1

471 et al. 2011) are used to provide initial and lateral meteorological boundary conditions for
472 an intermediate resolution run (grid spacing of 12 km, with use of convection
473 parameterizations) (Figure 3), which then provides driving boundary conditions for the
474 convection-permitting experiments. In the Texas case study, however, we nested the
475 model directly in the ERA-Interim reanalysis with boundary conditions provided every 6
476 hours, given that such configuration was able to reproduce accurately the HPE intensity.
477 In this case the model uses a large LBC relaxation zone which allows the description of
478 realistic fine-scale features driving this weather event (even if not fully consistent with the
479 Matte et al. (2017) criteria). All simulations start 24–48 hours before the HPE. The analysis
480 focuses on the total accumulated precipitation over the entire model domain at 3 km
481 resolution (Fig. 3) for the periods defined in Table 2. In the cases of California and Texas
482 the evaluation also includes the time series of 6 hourly accumulated precipitation
483 averaged on the region of maximum precipitation (black rectangles in Figs. 3) against
484 available high temporal resolution observations (NCEP/CPC) (Table 3). The discussion
485 of the case studies is presented in the next sections; the configuration files (namelists)
486 with full settings for the three test cases are available at
487 <https://zenodo.org/record/5106399>.

Deleted: 2

Deleted:

Deleted: In the Texas case study, we fed directly the fields from the ERA-Interim reanalysis to the RegCM 3km convection permitting simulation, because we found that the HPE intensity was already reproduced accurately with this procedure

Deleted: domains

Deleted: of

Deleted: 2

Deleted: and

Deleted: 1

Deleted: For

Deleted: 4

Deleted: ab

488
489 A key issue concerning the use of CP-RCMs is the availability of very high resolution,
490 high quality observed datasets for the assessment and evaluation of the models, which
491 is not there for most of the world regions. Precipitation measurements come from
492 essentially three distinct sources: in-situ rain-gauges, ground radar and satellite. In the
493 present study we use 7 observational datasets depending on the case study and the area
494 covered, as described in Table 2. We have used: Precipitation Estimation from Remotely
495 Sensed Information using Artificial Neural Networks - Climate Data Record (PERSIAN-
496 CDR), Climate Hazards Group InfraRed Precipitation with Station data (CHIRPS), the
497 Climate Prediction Center morphing method (CMORPH), Tropical Rainfall Measuring
498 Mission (TRMM), NCEP/CPC-Four Kilometer Precipitation Set Gauge and Radar
499 (NCEP/CPC), CPC-Unified daily gauge based precipitation estimates (CPC) and
500 Parameter-elevation Regressions on Independent Slopes Model (PRISM) (Table 3).
501 NCEP/CPC is a precipitation analysis which merges a rain gauge dataset with radar
502 estimates. CMORPH and PERSIAN-CDR are based on satellite measurements, CHIRPS
503 incorporates satellite imagery with in-situ station data. CPC is a gauge-based analysis of
504 daily precipitation and the PRISM dataset gathers climate observations from a wide range

520 of monitoring networks, applies sophisticated quality control measures, and develops
521 spatial climate datasets incorporating a variety of modeling techniques at multiple spatial
522 and temporal resolutions.

523

524

<u>Case</u>	<u>ACRONYM</u>	<u>Region of The event</u>	<u>Domains size</u> <u>lon x lat x vertical levels</u>	<u>Simulation Time Window</u>
1	CAL	California	480 x 440 x 41	15 Feb 2004 00:00 19 Feb 2004 00:00
2	TEX	Texas	480 x 440 x 41	9 June 2010 00:00 12 June 2010 00:00
3	LKV	Lake Victoria	550 x 530 x 41	25 Nov 1999 00:00 1 Dec 1999 00:00

525 **Table 2: List of acronyms and description of the test cases with corresponding 3km
526 domain sizes and simulation period.**

Deleted: and

<u>Dataset name</u>	<u>Region</u>	<u>Spatial Resolution</u>	<u>Temporal Resolution</u>	<u>Data Source</u>	<u>Reference</u>
TRMM	World	0.5°	Daily	Satellite	Huffman et al. (2007)
CHIRPS	World	0.05°	Daily	Station data+Satellite	Funk et al. (2015)
CMORPH	World	0.25°	Daily	Satellite	Joyce et al.

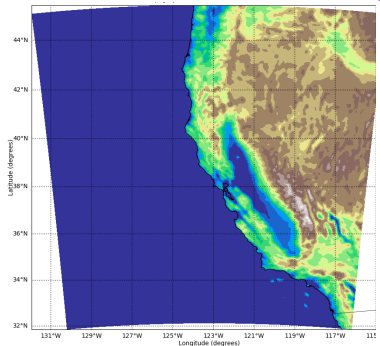
					(2004)
NCEP/CPC	USA	0.04°	Hourly	Gauge and Radar	https://doi.org/10.5065/D69Z93M3 . Accessed: 27/06/2018
CPC	World	0.5°	Daily	Station data	Chen and Xie (2008)
PRISM	USA	0.04°	Daily	Station data	PRISM Climate Group. 2016.
PERSIAN-CDR	World	0.25°	Daily	Satellite	Ashouri et al. (2015)

Table 3: List of observed precipitation datasets used for comparison.

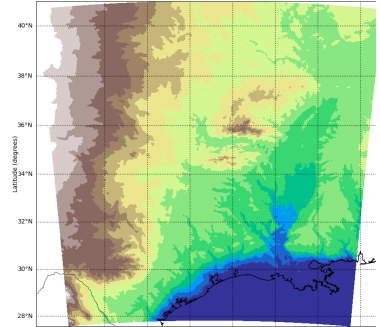
Deleted: gridded

Deleted: CAL (a)

Deleted: TEX (b)

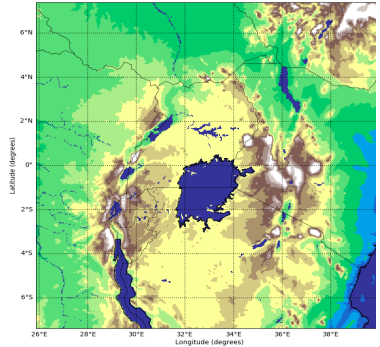


Deleted:

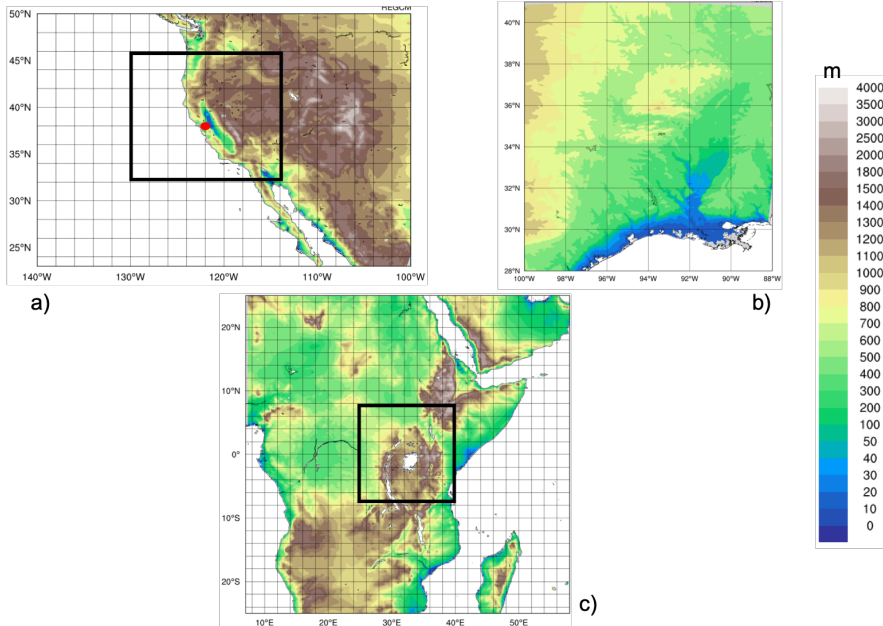


Deleted:

Deleted: LKV (c)



Deleted:



538
 539 **Figure 3: Simulation domains tested , a) California (CAL) , b) Texas (TEX), c) Lake**
 540 **Victoria (LKV) . For CAL (a) and LKV (b) the black square shows the 3 km simulation**
 541 **domains nested in the 12 km domain in figure. For TEX the 3 km domain simulation**
 542 **(c) is fed directly with the ERA-Interim reanalysis fields.**

543

544

545 California

546 The first case, referred to as CAL (California) in Table 2, is a HPE which occurred on 16–
 547 18 February 2004, producing flooding conditions for the Russian River, a southward-
 548 flowing river in the Sonoma and Mendocino counties of northern California (red-dot)
 549 (Figure 3). The event is documented in detail by Ralph et al. (2006), who focused their

Deleted: 2

Deleted: D

Deleted: 1

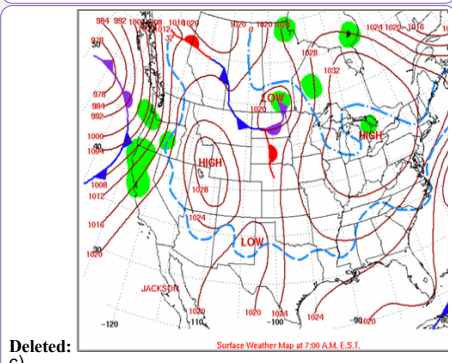
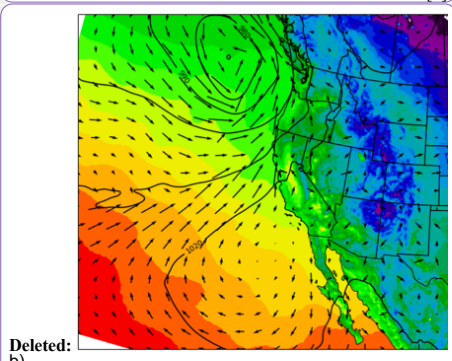
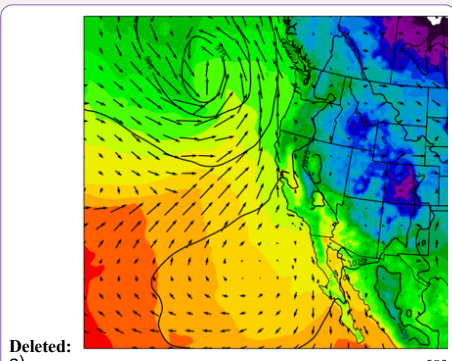
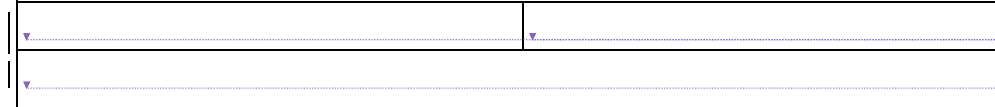
Deleted: in coastal

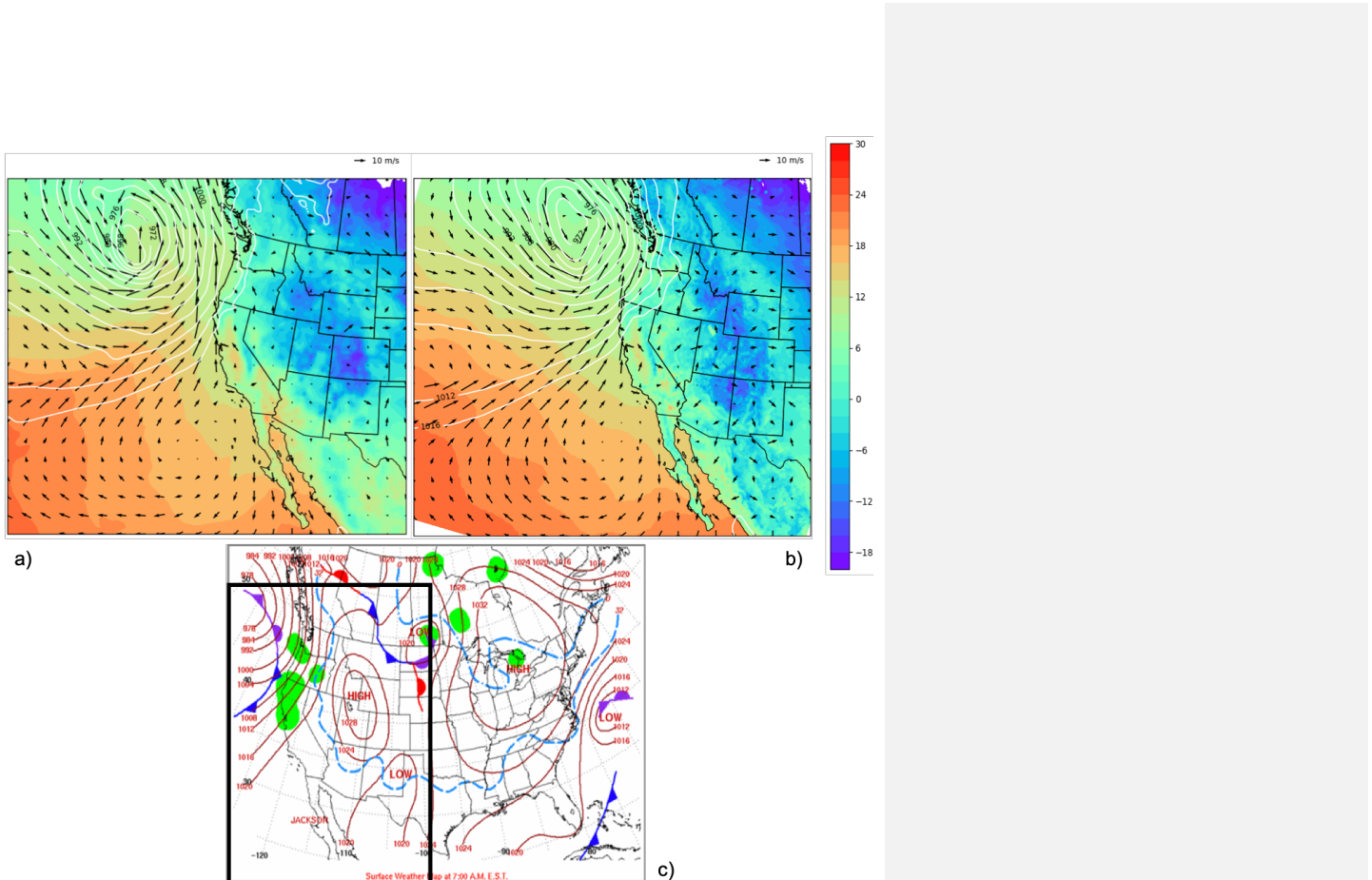
Deleted: f

Deleted: 2

566 attention on the impact of narrow filament-shaped structures of strong horizontal water
567 vapor transport over the eastern Pacific Ocean and the western U.S. coast, called
568 Atmospheric Rivers (ARs). ARs are typically associated with a low-level jet stream ahead
569 of the cold front of extratropical cyclones (Zhu and Newell 1998; Dacre et al. 2015; Ralph
570 et al. 2018), and can induce heavy precipitation where they make landfall and are forced
571 to rise over mountain chains (Gimeno et al. 2014). The CAL event consists of a slow
572 propagating surface front arching southeastward towards Oregon and then
573 southwestward offshore of California (Fig.3a,c). Rain began over the coastal mountains
574 of the Russian River watershed at 0700 UTC, 16 February, as a warm front descended
575 southward, and also coincided with the development of orographically favoured low-level
576 upslope flow Ralph et al. (2006).

567





578
 579 **Figure 4:** Mean sea level pressure (mslp) (white contour lines), surface temperature
 580 (color shading) and 100-m wind direction (black arrows) at 7:00 UTC, 16 Feb. 2004
 581 of ERA5 reanalysis (a) and RegCM 12km (b) respectively. (c) NCEP-NOA Surface
 582 Analysis of pressure and fronts. The black box in (c) bounded the area represented
 583 in (a) and (b)

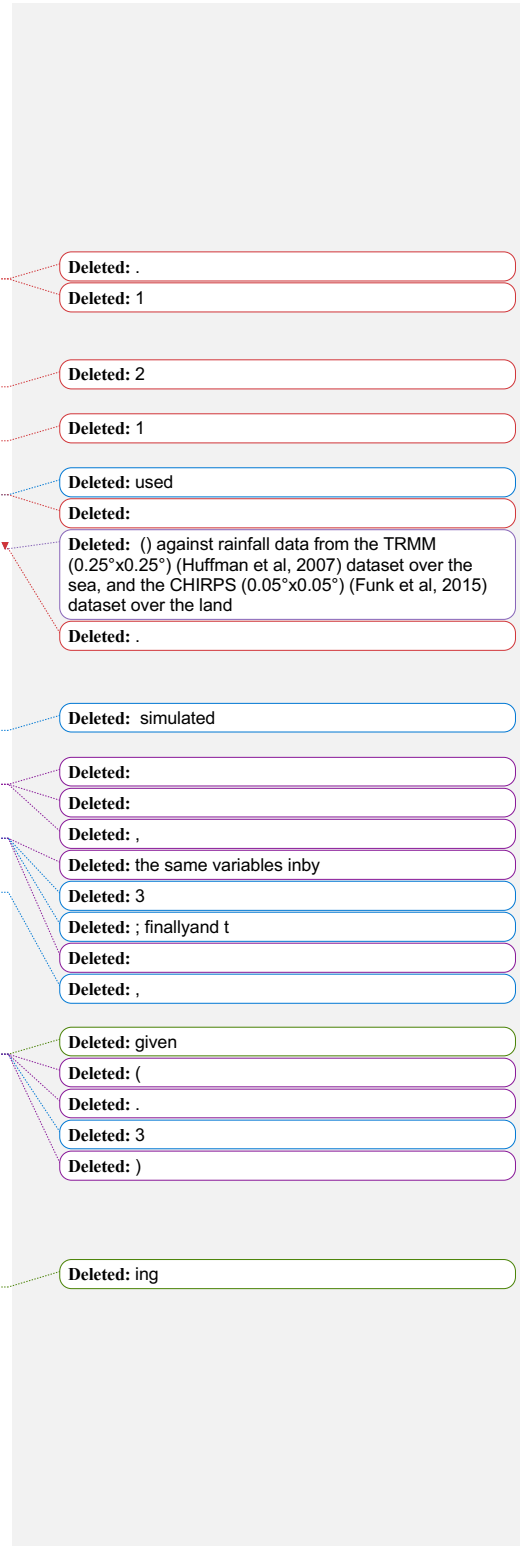
584 The intermediate resolution (12 km) domain Figure 3a covers a wide area
 585 encompassing California and a large portion of the coastal Pacific Ocean, with 23 vertical

Deleted: black

Deleted: f

Deleted: 2

589 levels and a parameterization for deep convection based on the Kain–Fritsch scheme
590 (Kain, 2004). The ERA-Interim driven simulation is initialized at 0000 UTC, 15 February
591 (Table 2) and lasts until 0000 UTC 19 February 2004. This simulation drives a
592 corresponding RegCM4-NH run using a smaller domain centered over northern California
593 (Fig. 3a) at 3 km horizontal grid spacing and 41 vertical levels, with boundary conditions
594 updated at 6 hour intervals. In RegCM4-NH only the shallow convection component of
595 the Tiedtke scheme (Tiedtke, 1996) is activated. Simulated precipitation is compared with
596 the CHIRPS, CMORPH, TRMM, PRISM, NCEP/CPC observations described in Table 3.
597 First, we notice that the synoptic conditions characteristic of this case study, which are
598 fed into the RegCM4-NH model, are well reproduced by RegCM4 at 12 km, as shown in
599 Figure 4, where we compare the mean sea level pressure (mslp), surface temperature
600 and wind direction on 14 Feb at 7:00 am, as simulated by RegCM at 12 km (Fig.3b) with
601 corresponding fields from the ERA5 reanalysis (Fig.4a). The surface analysis of pressure
602 and fronts derived from the operational weather maps prepared at the National Centers
603 for Environmental Prediction, Hydrometeorological Prediction Center, National Weather
604 Service (https://www.wpc.ncep.noaa.gov/dailywxmap/index_20040216.html) is also
605 reported in Figure 4c.
606 The observed precipitation datasets show similar patterns for the total accumulated
607 precipitation (Figure 5), in particular CHIRPS, PRISM and NCEP exhibit similar spatial
608 details and magnitudes of extremes. CHIRPS places a maximum around 42°N which is
609 not found in the other datasets. CMORPH and TRMM show lower precipitation maxima
610 and lesser spatial details due to their lower resolution, indicating that the performance of
611 satellite-based products may be insufficient as a stand alone product to validate the model
612 for this case.
613



640 In general, the observed precipitation datasets place the highest maxima on the terrain
641 peaks, with extreme rainfall greater than 250 mm in 60 hours over the coastal mountains
642 and greater than 100 – 175 mm elsewhere (Fig. 5a). The black box in Fig 5 shows the
643 area of the Russian River watershed, highlighting the locations of the observing systems,
644 including Cazadero (CZD) and Bodega Bay (BBY) where the largest rainfall rates were
645 detected ~~269 mm and 124 mm in 60-h accumulated rainfall between 0000 UTC 16~~
646 February and 1200 UTC 18 February 2004, respectively (Ralph et al., 2006).

647 The convection-permitting simulation captures the basic features of the observed
648 precipitation ~~as shown for example in Fig.5~~ both in terms of spatial distribution and
649 temporal evolution of rainfall (Fig.6a). However, it shows higher precipitation rates than
650 observed over the sea and over the mountain chains, with lower intensities than observed
651 in the south-east part of the mountain chain (Fig.5). By contrast, the 12-km simulation
652 severely underestimates the magnitude of the precipitation event (Fig.5).

653 Concerning the timing and intensity of the event in the CZD subregion, 6-hourly
654 accumulated precipitation (Fig.6a) averaged over the black box of Figure 5 shows that
655 both the 3 km and 12 km simulations capture the onset of the event, but the peak intensity
656 is strongly underestimated by the 12 km run, while it is well simulated by the 3 km run,
657 although the secondary maximum is overestimated. Therefore, our results demonstrate
658 that only the high resolution convection-permitting model captures ~~this~~ extreme event
659 and that parameterized convection has severe limits in this regard (Done et al. 2004; Lean
660 et al. 2008; Weisman et al. 2008; Weusthoff et al. 2010; Schwartz 2014; Clark et al. 2016).

661

Deleted: The

Deleted: elevation

Deleted: of

Deleted: in the domain

Deleted: 4

Deleted: 4

Deleted: .4a

Deleted: respectively

Deleted:

Deleted: (Fig.4a)

Deleted: 4

Deleted: g and 5a

Deleted: 5

Deleted: 4

Deleted: g

Deleted: 4

Deleted: d

Deleted: 5

Deleted: red

Deleted: 4

Deleted: a

Deleted: overall,

Deleted: show

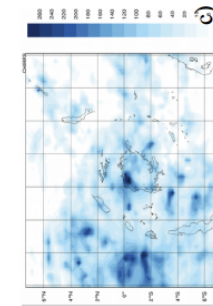
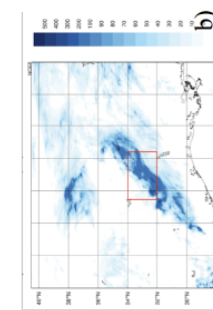
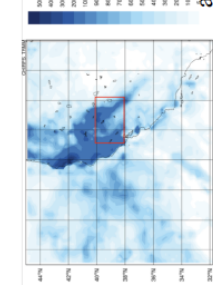
Deleted:

Deleted: ese

Deleted: s

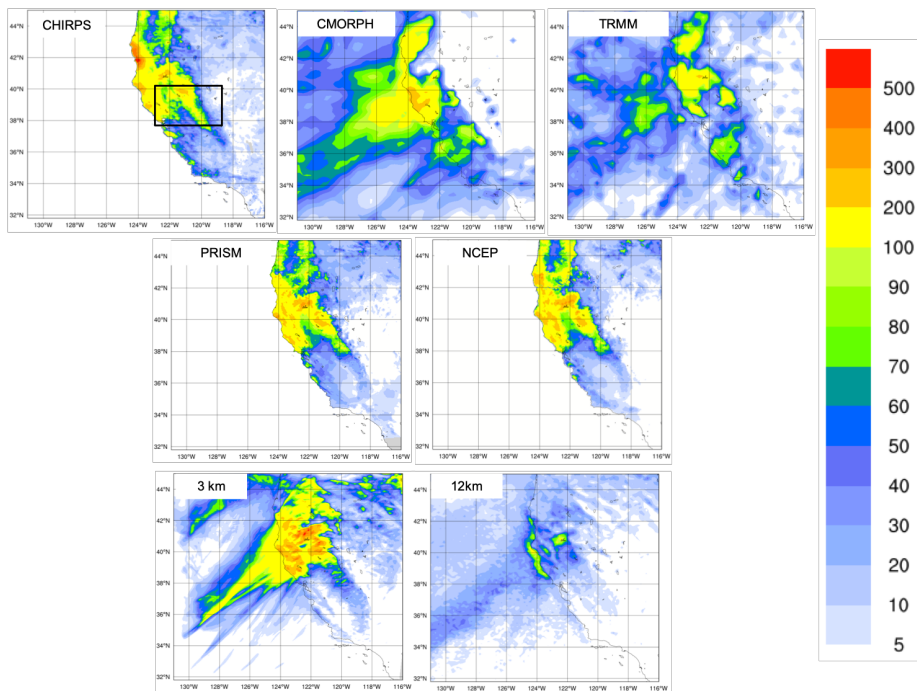
Total accumulated precipitation during the events (mm)

CAL TEX LKV



OBS 1

Deleted:

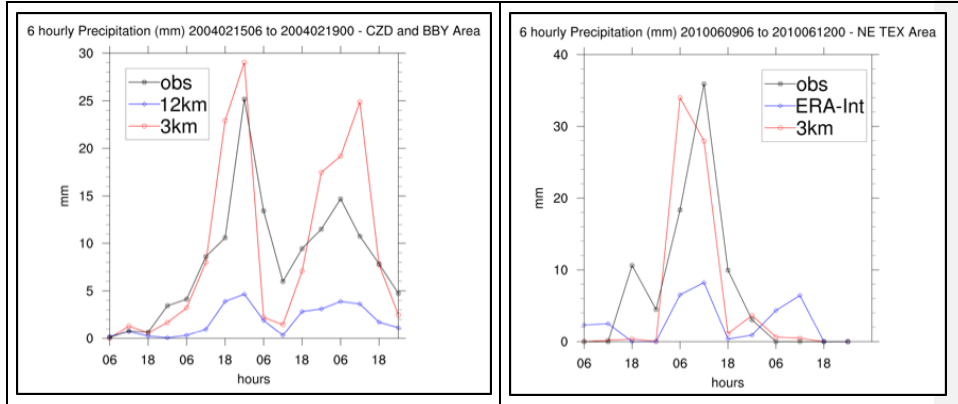


691
692 **Figure 5 :** Total accumulated precipitation (mm) during the California case:
693 CHIRPS, CMORPH, TRMM observations (top line), PRISM and NCEP Reanalysis
694 (middle line) and convection-permitting simulation with RegCM4-NH at 3km and
695 RegCM4 at 12km (bottom line) .The black box denotes the area where the spatial
696 average of 6-hourly accumulated precipitation is calculated and reported in Fig. 6.

Deleted: 4

Deleted: 5

CAL (a)	TEX (b)
---------	---------



700 **Figure 6:** Time series of the 6 hourly accumulated precipitation (in mm on the y-
 701 axis) during the CAL event (a) and during the TEX event (b). The blue lines show
 702 RegCM4 12 Km and ERA interim 6 hourly accumulated precipitation averaged over
 703 the areas indicated by the red square in Figure 3 (a,b) while the red line shows the
 704 6 hourly accumulated precipitation simulated by RegCM4-NH. The observations are
 705 shown with a black line.

Deleted: 5

Deleted: .

Deleted: 3 km

Deleted: in

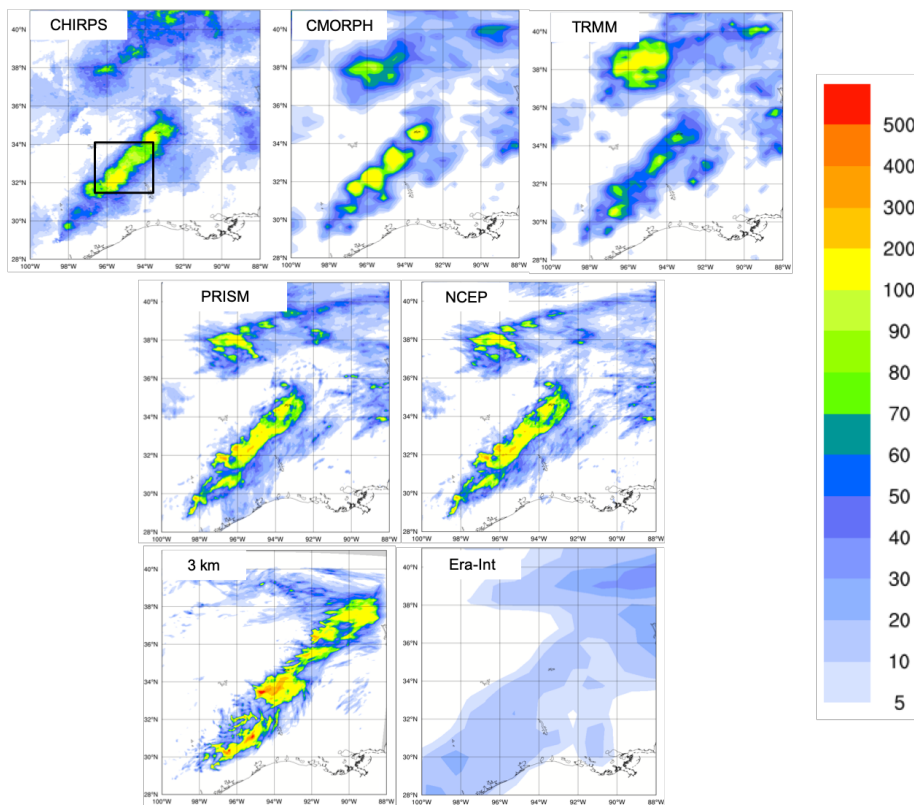
706

707 Texas

708 Case 2, hereafter referred to as TEX (Table 2), is a convective precipitation episode
 709 exhibiting characteristics of the “Maya Express” flood events, linking tropical moisture
 710 plumes from the Caribbean and Gulf of Mexico to midlatitude flooding over the central
 711 United States (Higgins 2011). During the TEX event, an upper-level cutoff low over
 712 northeastern Texas, embedded within a synoptic-scale ridge, moved slowly
 713 northeastward. Strong low-level flow and moisture transport from the western Gulf of
 714 Mexico progressed northward across eastern Texas. The event was characterized by
 715 low-level moisture convergence, weak upper-level flow, weak vertical wind shear, and

Deleted: 1

721 relatively cold air (center of cutoff low), which favored the slow-moving convective storms
722 and nearly stationary thunderstorm outflow boundaries. The main flooding event in
723 eastern Texas occurred on June 10, 2010, with a daily maximum rainfall of 216.4 mm of
724 the region in the [black](#) box of Figure 7. (Higgins 2011).



725
726 [Figure 7: Total accumulated precipitation \(mm\) during the Texas case: CHIRPS,](#)
727 [CMORPH, TRMM observations \(top line\), PRISM and NCEP Reanalysis \(central](#)
728 [line\) and convection-permitting simulation with RegCM4-NH at 3 km grid spacing](#)
729 [and Era-Int \(bottom line\). The black box shows the area where the spatial average](#)
730 [of 6-hourly accumulated precipitation was calculated and reported in Figure 6.](#)

Deleted: red
Deleted: grid
Deleted: 6
Deleted: 4b

Deleted: 6

Deleted: .5

737
738

739

740 As for the California case, the observed precipitation datasets show coherent patterns for
741 the total accumulated precipitation (Fig. 6), with the highest values related to the
742 mesoscale convective system in eastern Texas (~ 200 mm), and another smaller area of
743 high precipitation more to the north, approximately over Oklahoma. PRISM and NCEP
744 capture similar spatial details and magnitudes of extremes, CHIRPS has lower
745 precipitation extremes in the north compared to the other datasets, while CMORPH and
746 TRMM show the lowest precipitation extremes and reduced spatial details as already
747 noted for the California case.

748 The bottom panels in Figure 7 present precipitation as produced by the RegCM4-NH and
749 the ERA-Interim reanalysis (driving data), respectively. ERA-Interim reproduces some of
750 the observed features of precipitation, but with a substantial underestimation over the
751 areas of maximum precipitation because of its coarse resolution. By comparison, the
752 RegCM4-NH simulation (Fig. 7) shows an improvement in both pattern and intensity of
753 precipitation, and is substantially closer to observations over eastern Texas. However,
754 the precipitation area is slightly overestimated and the model is not capable of
755 reproducing the small region of maximum precipitation in the north.

756
757 The time series of precipitation over eastern Texas from 9 to 12 June 2010 for
758 observations (black line), ERA-Interim (blue line) and RegCM4-NH (red line) are reported
759 in Figure 6b. Precipitation increases over this region from 00:00, 10 June, until it reaches

Deleted: similar
Deleted: . In general the precipitation observations show (Fig. 6) ...
Deleted: with
Deleted: maximum
Deleted: amounts
Deleted: detects
Deleted: s
Deleted: .
Deleted: l
Deleted: dataset
Deleted: r
Deleted: less
Deleted: in general
Deleted: we
Deleted: In the daily precipitation observations for 10 June 2010 (NCEP stage-IV gridded precipitation, Fig. 4b) the highest values related to the mesoscale ... [91]
Deleted: Figures
Deleted: 6
Deleted: 4e and 4h
Deleted: show
Deleted: s
Deleted: reproduced
Deleted: the same information as in Figure 4b (bottom) [10]
Deleted: Era
Deleted: and the RegCM4-NH
Deleted: The
Deleted: shows
Deleted: n expected
Deleted: it also shows a
Deleted: pronounced
Deleted: , given its coarser resolution,
Deleted: s
Deleted: 4h
Deleted: are
Deleted: in the non-hydrostatic simulation
Deleted: (Figure 5b)
Deleted: shown
Deleted: F
Deleted: .
Deleted: 5

810 the observed maximum at 12:00, 10 June (~35 mm), gradually decreasing afterwards
811 until 6:00, 11 June. The RegCM4-NH simulation shows a more realistic temporal
812 evolution than the ERA-Interim, which exhibits an overall underestimation [of precipitation](#).
813 In general, the non-hydrostatic model produces precipitation values close to the
814 observations, however, the simulated maximum is reached 6 hours earlier than observed.

815
816

817 **Lake Victoria**

818 Case 3 focuses on Lake Victoria (LKV), with the purpose of testing RegCM4-NH on a
819 complex and challenging region in terms of convective rainfall. It is estimated that each
820 year 3,000-5,000 fishermen perish on the lake due to nightly storms (Red Cross, 2014).
821 In the Lake Victoria basin, the diurnal cycle of convection is strongly influenced by
822 lake/land breezes driven by the thermal gradient between the lake surface and the
823 surrounding land. As the land warms during the course of the day, a lake breeze is
824 generated which flows from the relatively cooler water towards the warmer land surface.
825 The circulation is effectively reversed at night, when the land surface becomes cooler
826 than the lake surface, leading to convergence over the lake and associated thermal
827 instability.

828 In the LKV region, prevailing winds are generally easterly most of the year with some
829 variability due to the movement of the ITCZ. The local diurnal circulation created by the
830 presence of the lake within the larger scale easterly wind field creates two diurnal rainfall
831 maxima. During daylight hours, when the lake breeze begins to advance inland,
832 convergence is maximized on the eastern coast of the lake as the lake breeze interacts
833 with the prevailing easterlies. Studies have also noted the importance of downslope

834 katabatic winds along the mountains to the east of the lake in facilitating convergence
835 along the eastern coastal regions (Anyah et al. 2006). This creates a maximum in rainfall
836 and convection on the eastern coast of LKV. Conversely, during nighttime hours, when
837 the local lake circulation switches to flow from the land towards the lake, the prevailing
838 easterlies create locally strong easterly flow across the lake and an associated maximum
839 in convergence and rainfall on the western side of LKV.

840 The LKV simulation starts on 25 November 1999 and extends to the beginning of
841 December 1999 (Table 2), covering a 5-day period which falls within the short-rain season
842 of East Africa. The choice of 1999, an ENSO neutral year, was made in order to focus the
843 analysis on local effects, such as the diurnal convection cycle in response to the lake/land
844 breeze, with no influence of anomalous large scale conditions. A 1-dimensional lake
845 model (Hostetler et al. 1993; Bennington et al. 2014) interactively coupled to RegCM4-
846 NH was utilized to calculate the lake surface temperature (LST), since lake-atmosphere
847 coupling has been shown to be important for the LKV (Sun et al. 2015; Song et al. 2004).
848 This coupled lake model has been already used for other lakes, including Lake Malawi in
849 southern Africa (Diallo et al. 2018). As with the other experiments, the boundary
850 conditions are provided by a corresponding 12 km RegCM4 simulation employing the
851 convection scheme of Tiedtke (1996).

852 At the beginning of the simulation, the LST over the lake is uniformly set to 26C, and is
853 then allowed to evolve according to the lake-atmosphere coupling. This initial LST value
854 is based on previous studies. For example, Talling (1969) finds Lake Victoria surface
855 temperatures ranging from 24.5-26°C during the course of the year. Several studies have
856 used RCMs to investigate the Lake Victoria climate (Anyia et al., 2006; Anyah and

Deleted: 1

858 Semazzi 2009, Sun et al. 2015), and found a significant relationship between lake
859 temperature and rainfall depending on season. The value of 26°C is typical of the winter
860 season and was chosen based on preliminary sensitivity tests using different values of
861 initial temperature ranging from 24°C to 26°C.

862 The synoptic feature favorable for the production of precipitation over the LKV in this
863 period corresponds to a large area of southeasterly flow from the Indian Ocean (Fig. 8a),
864 which brings low-level warm moist air into the LKV region facilitating the production of
865 convective instability and precipitation. This synoptic situation, with a low-level
866 southeasterly jet off the Indian Ocean, is a common feature associated with high
867 precipitation in the area (Anyah et al. 2006) is found in ERA5 (Figure 7a).

868

a)

b)

Deleted: is initial LST value was chosen based on preliminary simulations and was shown to produce the most realistic precipitation for the period compared with CMORPH (Joyce et al., 2004)

Deleted: 7

Deleted: 6

Deleted: This southeasterly flow

Deleted:

Deleted: es

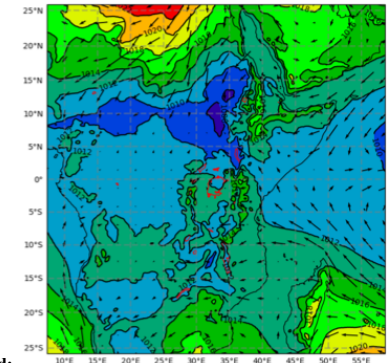
Deleted: etup

Deleted:

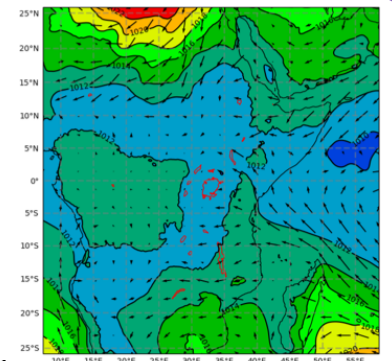
Deleted: production

Deleted: LKV region

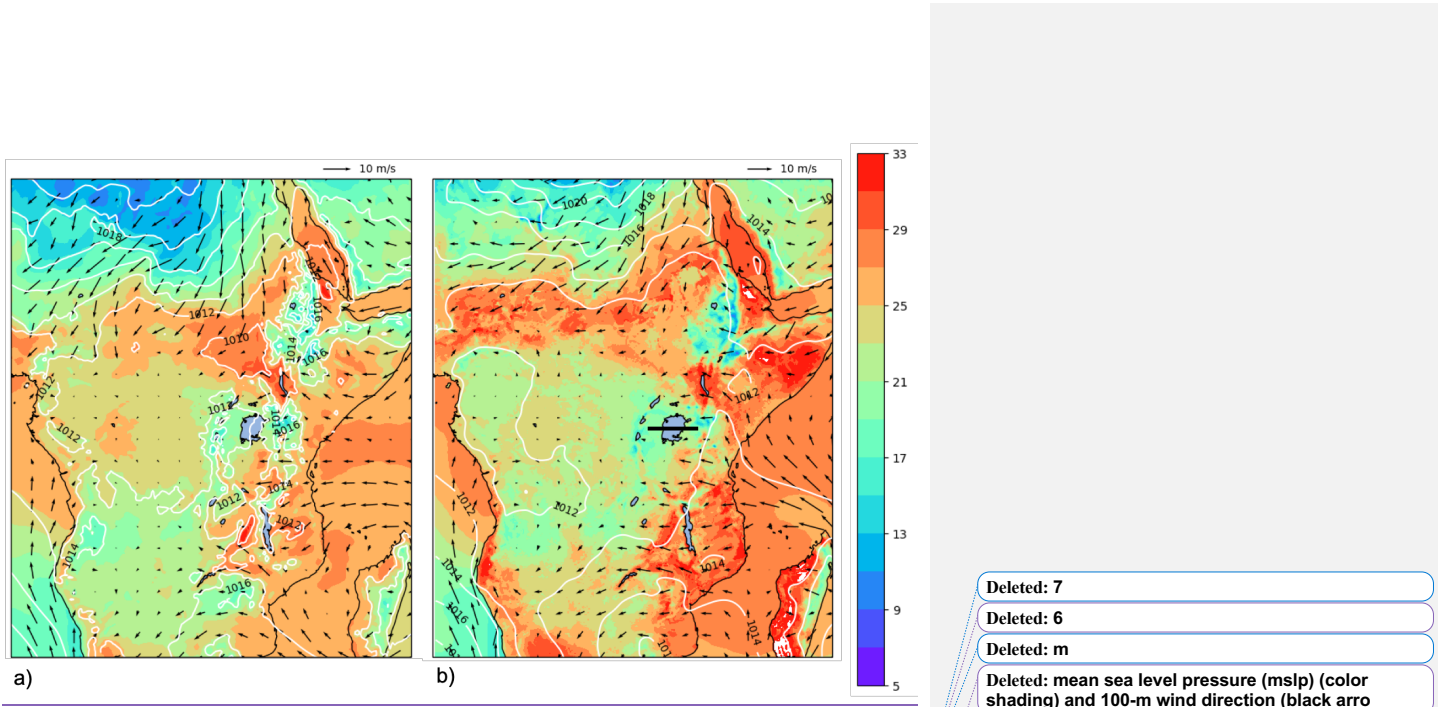
Deleted: 6



Deleted:



Deleted:



885 **Figure 8:** Mean sea level pressure (mslp) (white black contour lines), surface
 886 temperature (color shading) and 100-m wind direction (black arrows), averaged over
 887 the period 25 November 00:00 - 1 December 00:00, of ERA5 reanalysis (a) and
 888 RegCM 12km (b). The black line (b) shows the cross-section position represented
 889 in Fig. 9

Deleted: 7
 Deleted: 6
 Deleted: m
 Deleted: mean sea level pressure (mslp) (color shading) and 100-m wind direction (black arrows)
 Deleted: averaged over the period
 Deleted: 9
 Deleted: 2
 Deleted: The Victoria Lake and the others lakes in the domain are highlighted in red line
 Formatted: Font: 12 pt
 Deleted: 8
 Deleted: 7
 Deleted: o
 Deleted: o
 Deleted: bottom
 Deleted: 9
 Deleted: o
 Deleted: convection
 Deleted: 8
 Deleted: 7
 Deleted: a
 Deleted: 4
 Deleted: during strong
 Deleted: 8
 Deleted: 7
 Deleted: b
 Deleted: 3

891
 892 The LKV region dynamics are quite distinct between nighttime and daytime and the
 893 rainfall in and around the lake has a pronounced diurnal cycle. To understand this strong
 894 diurnal cycle, Figure 9 shows a cross-section through the lake (32E to 34E, black line in
 895 right panel of Fig. 8) along 1S latitude at a period during strong nighttime (Fig. 9b,d; 6Z
 896 30 November) and daytime convection (Fig. 9a,c; 12Z 29 November). During the day,

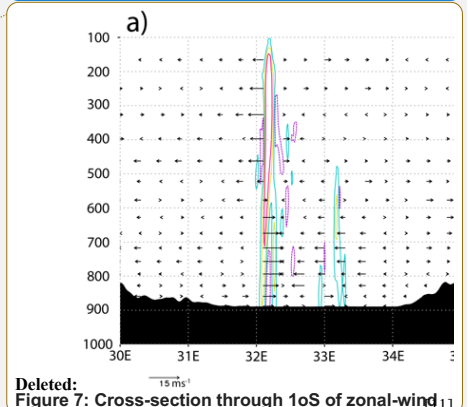
924 surface heating around the lake leads to a temperature differential between the land and
925 lake sufficient to generate, a lake breeze, which causes divergence over the lake, while
926 over the surrounding highlands the environment is more conducive to convection (9a,c).

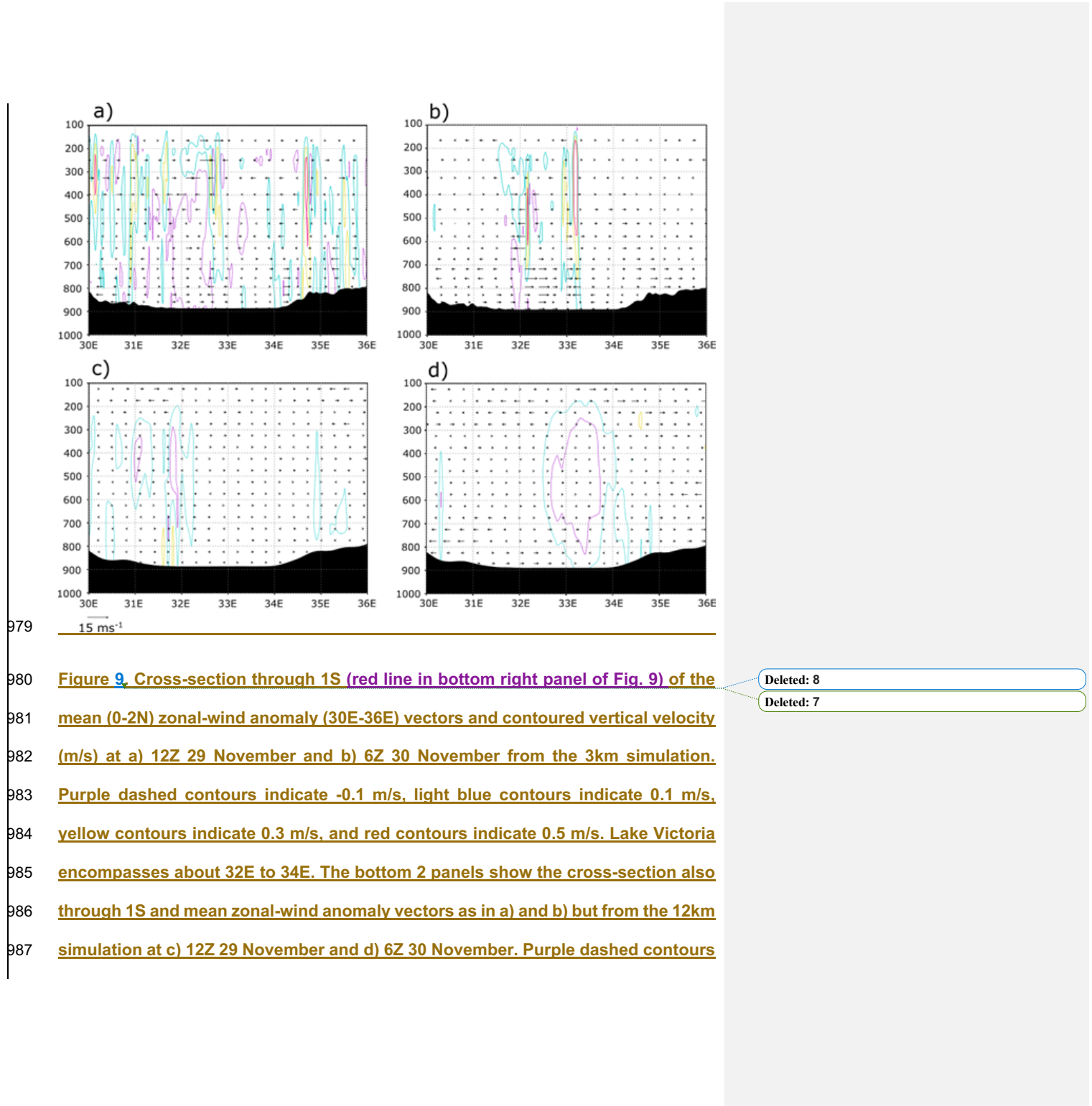
927 Conversely, during the night, a land breeze circulation is generated, which induces
928 convergence and convection over the lake, (Figure 9b,d).

929 Comparing the 3 km simulation to the 12 km forcing run, we find that the localized
930 circulations created by local forcings (i.e. convection) are much stronger in the high
931 resolution experiment. We also find stronger and more localized areas of convective
932 updrafts as seen in the vertical velocities (9a,b) compared to the 12 km simulation (8c,d);
933 omega is shown instead of vertical velocity here because of the difference in model
934 output). The stronger convection simulated in the 3 km experiment is also tied to the
935 stronger temperature gradients between lake and land and between day and night, (Figure
936 10).

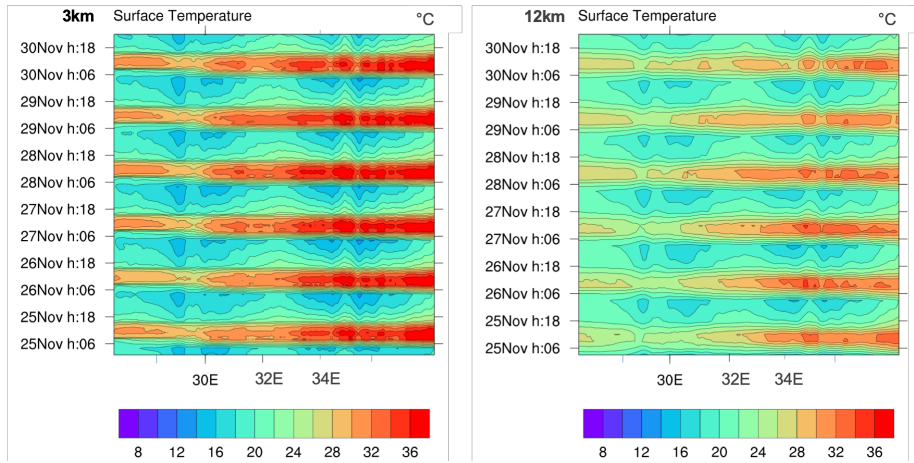
937 This demonstrates that the 3km simulation is better equipped to simulate the localized
938 circulations associated with this complex land-lake system.

Deleted: create
Deleted: . This lake breeze promotes
Deleted: 8
Deleted: 7
Deleted: is in opposition to the large scale easterly flow over the region and consequently strong convergence and convection is maximized in the highlands to the east of the lake (Fig.).
Deleted: the lake becomes the focus of
Deleted: and consequently a focus for
Deleted: as seen in
Deleted: 8
Deleted: 7
Deleted: a
Deleted: simulation
Deleted: 3km simulation
Deleted: 8
Deleted: 7
Deleted: 7
Deleted: st
Deleted: /
Deleted: /
Deleted: represented in the 3km simulation compared to than in the 12 km one, as shown in
Deleted: f
Deleted: 9
Deleted: 8
Deleted: by the Longitude-time (hourly) Hovmöller diagram of LKV domain surface temperature.





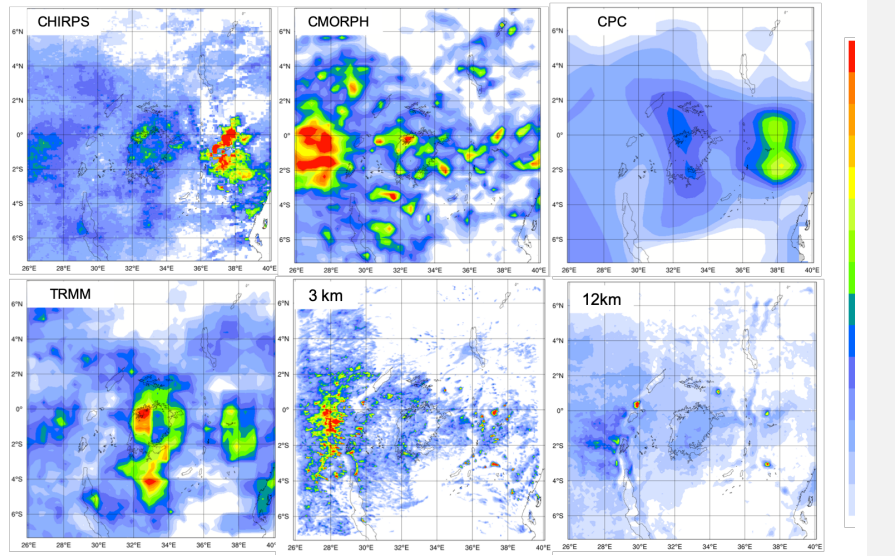
990 indicate -0.01 hPa/s, light blue dashed contours indicate -0.005 hPa/s, and yellow
991 dashed contours indicate 0.005 hPa/s.



993 Figure 10 : Longitude-time (hourly) Hovmöller diagram of LKV domain surface
994 temperature (shading, in °C). Panels correspond to the 3km simulation (left) and
995 12km simulation (right). The lake Victoria is between 32E and 34E longitude

Deleted: 9

Deleted: 8



998
999 **Figure 11:** Total accumulated precipitation during the LKV case measured by
1000 CHIRPS (top left), CMORPH (top center), CPC (top right) TRMM (bottom left) and
1001 calculated by RegCM4 at 3 km (bottom center) and 12 km (bottom right).
1002

1003 Figure 11 finally reports the total accumulated precipitation observed and simulated for
1004 the LKV case. TRMM and CPC show a similar pattern, with two-rainfall maxima of
1005 different intensities over the southeastern and northwestern lake areas. CMORPH shows
1006 a western rainfall maximum similar to TRMM and one large rainfall area almost entirely
1007 centered over the highlands to the west of the lake. Conversely in CHIRPS, a maximum
1008 is found to the east of the lake while several localized maxima occur over the lake. The
1009 differences between the observed datasets highlight the issue of observational
1010 uncertainty and the need to take into consideration shortcomings associated with the
1011 types of observational datasets considered. Different datasets can have significantly

Deleted: 9

Deleted: 0

Deleted: 9

Deleted: 4c

Deleted: shows

Deleted: measured

Deleted: for the total accumulated precipitation

Deleted: and the northwestern lake

Deleted: -area rainfall concentration, which is

Deleted: shows

Deleted: over the lake

Deleted: tself

Deleted: are seen

1b25 different climatology, especially in areas of low data availability. For example, Prein and
1026 Gobiet (2017) analyzed two gauge-based European-wide datasets, and seven global low-
1027 resolution datasets, and found large differences across the observation products, often
1028 of similar magnitude as the difference between model simulations. In this case and for
1029 this area the observation uncertainty plays a big role especially at high resolution, and
1030 highlights the need for an adequate observational network for model validation.

1031 However, even taking into account the elevated uncertainty existing in the observations
1032 datasets, we find a significant underestimation of rain amounts in the 12 km run (Fig 11),
1033 with a wide area of rainfall around 80mm over the whole of LKV. In contrast, the 3 km
1034 simulation shows substantially greater detail, with rainfall patterns more in agreement with
1035 the CMORPH observations. In particular, the 3 km simulation reproduces well the local
1036 rainfall maxima on the western side of the lake, although these appear more localized
1037 and with a multi-cell structure compared to CMORPH and TRMM. Additionally, the 12
1038 km simulation underestimates the observed heavy rainfall totals in the highlands to the
1039 west of the lake region, which are instead reproduced by the 3 km simulation.

1040 This last test case demonstrates the ability of RegCM4-NH in simulating realistic
1041 convective activity over a morphologically complex region, which is a significant
1042 improvement compared to the hydrostatic-coarse resolution model configuration.

1044 Conclusions and future outlook

1045 In this paper we have described the development of RegCM4-NH, a non hydrostatic
1046 version of the regional model system RegCM4, which was completed in response to the
1047

Deleted: variability between
Deleted: demonstrating that the spread of observation datasets from different sources are often compar
Deleted: such
Deleted: s
Deleted: essential
Formatted: Font:
Formatted: Font: Highlight
Deleted: shows that the total observed rainfall for the period is characterized by diurnal rainfall maxima associated with the local lake circulation. In particular, the north-western side of the lake shows a rainfall maximum exceeding 250mm during the 5-day simulation, while most of the north-west portion of the lake shows over 150mm in total rainfall. In addition, a weaker but still significant rainfall maximum is seen on the inland south-eastern coast of LKV.
Deleted: for this case
Deleted: Comparing the 12 km simulated rainfall (Fig. 9 4f) to the 3 km simulation (Fig. 94i),
Deleted: significantly
Deleted: less
Deleted: former
Deleted: significantly more localization of the
Deleted: which and this is
Deleted: ed amount
Deleted: otals
Deleted: (observed in most dataset with different intensities)...
Deleted: , which show the highest observed peak.
Deleted: In particular, the 3 km simulation reproduces 121
Deleted: is unable to produce
Deleted: with a strong underestimation
Deleted: whereas these are well captured in
Deleted: In summary, overall also Tt
Deleted: that
Deleted: the
Deleted: robust
Deleted: this
Deleted: and that
Deleted: is found
Deleted: with respect
Deleted: r
Deleted: and hydrostatic
Deleted: s

1096 need of moving to simulations at convection-permitting resolutions of a few km. The
1097 dynamical core of the non-hydrostatic version of MM5 has been thus incorporated into
1098 the RegCM4 system, an approach facilitated by the fact that the this last is essentially an
1099 evolution of the MM5. Some modifications to the MM5 dynamical core were also
1100 implemented to increase the model stability for long term runs. RegCM4-NH also includes
1101 two explicit cloud microphysics schemes needed to explicitly describe convection and
1102 cloud processes in the absence of the use of cumulus convection schemes. Finally, we
1103 presented a few case studies of explosive convection to illustrate how the model provides
1104 realistic results in different settings and general improvements compared to the coarser
1105 resolution hydrostatic version of RegCM4 for such types of events.

1106
1107 As already mentioned, RegCM4-NH is currently being used for different projects, and
1108 within these contexts, is being run at grid spacings of a few km for continuous decadal
1109 simulations, driven by reanalyses of observations or GCM boundary conditions (with the
1110 use of an intermediate resolution domains) over different regions, such as the Alps, the
1111 Eastern Mediterranean, Central-Eastern Europe and the Carribbeans. These projects,
1112 involving multi-model intercomparisons, indicate that the performance of RegCM4-NH is
1113 generally in line with that of other convection permitting models, and exhibits similar
1114 improvements compared to coarser resolution models, such as a better simulation of the
1115 precipitation diurnal cycle and of extremes at hourly to daily time scales. The results
1116 obtained within the multi-model context confirm previous results from single-model
1117 studies (Kendon et al. 2012, 2017, Ban et al. 2014, 2015; Prein et al. 2015, 2017), but
1118 also strengthen the robustness of the findings through reduced uncertainty compared to
1119 coarse resolution counterpart (Ban et al., 2021, Pichelli et al., 2021). The convection-
1120 permitting scale can thus open the perspective of more robust projections of future
1121 changes of precipitation, especially over short time scales.

1122
1123
1124 One of the problems of the RegCM4-NH dynamical core is that, especially for long runs
1125 with varied meteorological conditions, a relatively short time step needs to be used for
1126 stability reasons. This makes the model rather computationally demanding, although not

Deleted: Towards this goal we have incorporated into the RegCM4 framework Tt

Deleted: from

Deleted: RegCM system

Deleted: , as described in section 2

Deleted: RegCM4-NH is currently being used for different projects, such as the Flagship Pilot Study on convection permitting modeling (Coppola et al. 2020, Ban et al. 2021, Pichelli et al. 2021) and the EUCLP EU project (Hewitt and Lowe 2018). In these contexts, the model is being run at grid spacings of a few km for continuous decadal simulations, both driven by reanalyses of observations and GCM fields (in both cases with the use of an intermediate resolution run to act as interface) over different regions, such as the Alps, the Eastern Mediterranean, Central-Eastern Europe and the Carribbeans. This will help better validate and understand the model behavior at these high resolutions....

1146 more than other convection-permitting modeling systems such as the Weather Research
1147 and Forecast model (WRF, Skamarok et al. 2008). For this reason, we are currently
1148 incorporating within the RegCM system a very different and more computationally efficient
1149 non-hydrostatic dynamical core, which will provide the basis for the next version of the
1150 model, RegCM5, to be released in the future.

1151

1152 Following the philosophy of the RegCM modeling system, RegCM4-NH is intended to be
1153 a public, free, open source community resource for external model users. The non-
1154 hydrostatic dynamical core has been implemented in a way that it can be activated, in
1155 place of the hydrostatic dynamics, through a user-set switch, which makes the use of
1156 RegCM4-NH particularly simple and flexible. We therefore envision that the model will be
1157 increasingly used by a broad community so that a better understanding can be achieved
1158 of its behavior, advantages and limitations.

1159

1160 **Code availability:** <https://zenodo.org/record/4603556>

1161 **Cases study configuration files:** <https://zenodo.org/record/5106399>

1162

1163

1164 **Author contribution:** CE prepared the manuscript with contributions from all co-authors
1165 and coordinated research, SP, TA, GR carried out and analysed the simulations, PE
1166 investigated solutions to stabilize/adapt the model at the km-scale and performed
1167 preliminary validation tests, GG developed/adapted the model code, FDS contributed to
1168 develop the coupled version of the model, NR developed one of the microphysics
1169 scheme, GF supervised and coordinated all activities.

1170

1171 **Competing interests:** The authors declare that they have no conflict of interest.

1172

1173

1174 **References**

1175 Anyah, R., Semazzi, F. H. M., Xie, L., 2006: Simulated Physical Mechanisms Associated
1176 with Climate Variability over Lake Victoria Basin in East Africa, *Mon. Wea. Rev.*, 134
1177 3588-3609.

1178

Deleted:

Deleted: ,

Deleted: ,

Formatted: Font: Bold

1182 Anthes, R. A., Hsie, E. -Y., & Kuo, Y. -H. (1987). Description of the Penn State/NCAR
1183 Mesoscale Model: Version 4 (MM4) (No. NCAR/TN-282+STR). doi:10.5065/D64B2Z90
1184
1185 Anyah, R. O., F. H. M. Semazzi, L. Xie, 2006: Simulated Physical Mechanisms
1186 Associated with Climate Variability over Lake Victoria Basin in East Africa. *Mon. Wea.
1187 Rev.*, 134, 3588-3609.,
1188
1189 [Anyah RO, Semazzi F \(2009\) Idealized simulation of hydrodynamic characteristics of
1190 Lake Victoria that potentially modulate regional climate. *Int J Climatol* 29\(7\):971–981.
1191 doi:10.1002/joc.1795](#)
1192
1193 [Ashouri, Hamed, Kuo Lin Hsu, Soroosh Sorooshian, Dan K. Braithwaite, Kenneth R.
1194 Knapp, L. Dewayne Cecil, Brian R. Nelson and Olivier P. Prat \(2015\). 'PERSIANN- CDR:
1195 Daily precipitation climate data record from multisatellite observations for hydrological and
1196 climate studies'. In: *Bulletin of the American Meteorological Society*. ISSN: 00030007.
1197 DOI: 10.1175/BAMS-D-13-00068.1.](#)
1198

1199 Ban, N., J. Schmidli, and C. Schär, 2014: Evaluation of the convection-resolving regional
1200 climate modeling approach in decade-long simulations. *J. Geophys. Res. Atmos.*, 119,
1201 7889– 7907, <https://doi.org/10.1002/2014JD021478>.
1202
1203 Ban N, Schmidli J, Schär C (2015) Heavy precipitation in a changing climate: does short-
1204 term summer precipitation increase faster? *Geophys Res Lett* 42:1165–1172.
1205 <https://doi.org/10.1002/2014GL062588>
1206 Ban, N., Caillaud, C., Coppola, E. *et al.* The first multi-model ensemble of regional climate
1207 simulations at kilometer-scale resolution, part I: evaluation of precipitation. *Clim Dyn*
1208 (2021). <https://doi.org/10.1007/s00382-021-05708-w>
1209
1210 Beheng, K.: A parameterization of warm cloud microphysical conversion processes,
1211 *Atmos. Res.*, 33, 193–206, 1994

1212

1213 Bennington V, Notaro M, Holman KD, 2014: Improving Climate Sensitivity of Deep Lakes
1214 within a Regional Climate Model and Its Impact on Simulated Climate, *J. Climl*, 27, 2886-
1215 2911.

1216

1217 [Bretherton CS, McCaa JR, Grenier H \(2004\) A new parameterization for shallow cumulus](#)
1218 [convection and its application to marine subtropical cloud-topped boundary layers. I.](#)
1219 [Description and 1D results. Mon Weather Rev 132: 864– 882.](#)

1220

1221 Chan, S. C., E. J. Kendon, H. J. Fowler, S. Blenkinsop, N. M. Roberts, and C. A. T. Ferro,
1222 2014: The value of high- resolution Met Office regional climate models in the simulation
1223 of multi-hourly precipitation extremes. *J. Climate*, 27, 6155–6174,
1224 <https://doi.org/10.1175/JCLI-D-13-00723.1>.

1225

1226 [Chen, Mingyue and Pingping Xie \(2008\). 'CPC Unified Gauge-based Analysis of Global](#)
1227 [Daily Precipitation'. In: 2008 Western Pacific Geophysics Meeting. ISBN: 0026- 0576.](#)
1228 [DOI: http://dx.doi.org/10.1016/S0026-0576\(07\)80022-5.](http://dx.doi.org/10.1016/S0026-0576(07)80022-5)

1229

1230

1231 Clark, P., N. Roberts, H. Lean, S. P. Ballard, and C. Charlton- Perez, 2016: Convection-
1232 permitting models: A step-change in rainfall forecasting. *Meteor. Appl.*, 23, 165–181,
1233 <https://doi.org/10.1002/met.1538>.

1234

1235 [Coppola, E., Sobolowski, S., Pichelli, E. et al. A first-of-its-kind multi-model convection](#)
1236 [permitting ensemble for investigating convective phenomena over Europe and the](#)
1237 [Mediterranean. *Clim Dyn* 55, 3–34 \(2020\). https://doi.org/10.1007/s00382-018-4521-8](#)

1238

1239 [Coppola E, Giorgi F, Mariotti L, Bi X \(2012\) RegT-Band: a tropical band version of](#)
1240 [RegCM4. *Clim Res* 52: 115–133](#)

1241

Deleted: 

Deleted: <https://doi.org/10.1175/JCLI-D-13-00723.1>

1244 Dacre, H. F., P. A. Clark, O. Martinez-Alvarado, M. A. Stringer, and D. A. Lavers, 2015:
1245 How do atmospheric rivers form? Bull. Amer. Meteor. Soc., 96, 1243-1255,
1246 <https://doi.org/10.1175/BAMS-D-14-00031>.

1247 Dale, M., A. Hosking, E. Gill, E. J. Kendon, H. J. Fowler, S. Blenkinsop, and S. C. Chan,
1248 2018: Understanding how changing rainfall may impact on urban drainage systems; les-
1249 sons from projects in the UK and USA. Water Pract. Technol., 13, 654–661,
1250 <https://doi.org/10.2166/wpt.2018.069>.

1251

1252 Diallo, I., Giorgi, F. and Stordal, F. (2018) Influence of Lake Malawi on regional climate
1253 from a double nested regional climate model experiment. Climate Dynamics, 50, 3397–
1254 3411. <https://doi.org/10.1007/s00382-017-3811-x>

1255

1256 Dickinson, R.E., Errico, R.M., Giorgi, F. et al. A regional climate model for the western
1257 United States. Climatic Change 15, 383–422 (1989). <https://doi.org/10.1007/BF00240465>

1258

1259 [Dickinson RE, Henderson-Sellers A, Kennedy P \(1993\) Bio -sphere– atmosphere transfer](#)
1260 [scheme \(BATS\) version 1eas coupled to the NCAR community climate model. TechRep.](#)
1261 [National Center for Atmospheric Research TechNote NCAR.TN-387+ STR, NCAR,](#)
1262 [Boulder, CO](#)

1263

1264 Done, J., C. A. Davis, and M. L. Weisman, 2004: The next gener- ation of NWP: Explicit
1265 forecasts of convection using the Weather Research and Forecasting (WRF) model.
1266 Atmos. Sci. Lett., 5, 110–117, <https://doi.org/10.1002/asl.72>.

1267

1268 Dudhia, J., 1989: Numerical study of convection observed during the winter monsoon
1269 experiment using a mesoscale two-dimensional model, J. Atmos. Sci., 46, 3077–3107.

1270

1271 Durran D.R. and Klemp J.B.: A compressible model for the simulation of moist mountain
1272 waves, Mon. Wea. Rev., 111, 2341–236, 1983.

1273

Deleted: <https://doi.org/10.1007/BF00240465>

1275 Elguindi N., Bi X., Giorgi F., Nagarajan, B. Pal J., Solmon F., Rauscher S., Zakey S.,
1276 O'Brien T., Nogherotto R. and Giuliani G., 2017: Regional Climate Model
1277 RegCMReference ManualVersion 4.7, 49 pp, <https://zenodo.org/record/4603616>

Deleted: <https://zenodo.org/record/4603616>

1279 [Emanuel KA \(1991\) A scheme for representing cumulus convection in large-scale](#)
1280 [models. J Atmos Sci 48:2313–2335](#)

1282 [Fairall, C.W., E.F. Bradley, J.S. Godfrey, G.A. Wick, J.B. Edson, and G.S. Young, 1996a: The cool skin and the warm layer in bulk flux calculations. J. Geophys. Res. 101, 1295–1308.](#)

1286 [Fairall, C.W., E.F. Bradley, D.P. Rogers, J.B. Edson, G.S. Young, 1996b: Bulk parameterization of air-sea fluxes for TOGA COARE. J. Geophys. Res. 101, 3747–3764.](#)

Formatted: Font: (Default) Arial, 12 pt

1289 Funk, C., Peterson, P., Landsfeld, M. et al. The climate hazards infrared precipitation with
1290 stations—a new environmental record for monitoring extremes. Sci Data 2, 150066
1291 (2015). <https://doi.org/10.1038/sdata.2015.66>

1293 Gimeno, L., R. Nieto, M. Vásquez, and D. A. Lavers, 2014: Atmospheric rivers: A mini-review. Front. Earth Sci., 2, <https://doi.org/10.3389/feart.2014.00002>.

1295
1296 Giorgi F (2019) Thirty years of regional climate modeling: where are we and where are
1297 we going next? J Geophys Res Atmos 124:5696–5723

1298
1299 [Giorgi F, Coppola E, Solmon F, Mariotti L and others \(2012\) RegCM4: model description](#)
1300 [and preliminary tests over multiple CORDEX domains. Clim Res 52:7–29.](#)
1301 <https://doi.org/10.3354/cr01018>

Deleted: Giorgi F et al (2012) RegCM4: model description and preliminary tests over multiple CORDEX domains. Clim Res 52:7–29

1309 [Giorgi F, Francisco R, Pal JS \(2003\) Effects of a sub-gridscale topography and landuse](#)
1310 [scheme on surface climate and hydrology. I. Effects of temperature and water](#)
1311 [vapordisaggregation. J Hydrometeorol 4: 317– 333](#)
1312
1313 Giorgi F, Jones C, Asrar G (2009) Addressing climate information needs at the regional
1314 level: the CORDEX framework. WMO Bull 175–183
1315
1316 Giorgi F, Mearns LO (1999) Introduction to special section: regional climate modeling
1317 revisited. J Geophys Res 104:6335–6352
1318
1319 [Giorgi F, Marinucci MR, Bates G \(1993a\) Development of a second generation regional](#)
1320 [climate model \(RegCM2\). I. Boundary layer and radiative transfer processes.](#)
1321 [MonWeather Rev 121: 2794–2813](#)
1322
1323 Giorgi F, Marinucci MR, Bates G, DeCanio G (1993b) Development of a second
1324 generation regional climate model (RegCM2), part II: convective processes and
1325 assimilation of lateral boundary conditions. Mon Weather Rev 121:2814–2832
1326
1327 Giorgi, F., and G. T. Bates, 1989: The Climatological Skill of a Regional Model over
1328 Complex Terrain. Mon. Wea. Rev., 117, 2325–2347, [https://doi.org/10.1175/1520-0493\(1989\)117<2325:TCSOAR>2.0.CO;2](https://doi.org/10.1175/1520-0493(1989)117<2325:TCSOAR>2.0.CO;2).
1329
1330 G. A. Grell, J. Dudhia and D. R. Stauffer, “A Description of the Fifth Generation Penn
1331 State/NCAR Mesoscale Model (MM5),” NCAR Tech. Note, NCAR/TN-398+STR,
1332 Boulder, 1995, p. 122.
1333
1334 [Grell GA \(1993\) Prognostic evaluation of assumptions used by cumulus](#)
1335 [parameterizations. Mon Weather Rev 121: 764– 787](#)
1336
1337 [Grell, G., A.J. Dudhia, and D.R. Stauffer, 1994, A description of the fifth-generation Penn](#)
1338 [State/NCAR mesoscale model \(MM5\). NCAR Technical Note, NCAR/TN- 398+STR.](#)
1339

1340 Gunn, K. L. S., and J. S. Marshall, 1958: The distribution with size of aggregate
1341 snowflakes. *J. Meteor.*, 15, 452–461, [https://doi.org/10.1175/1520-0469\(1958\)015<0452:TDWSOA>2.0.CO;2](https://doi.org/10.1175/1520-0469(1958)015<0452:TDWSOA>2.0.CO;2).

1343

1344 Gutowski Jr., W. J., Giorgi, F., Timbal, B., Frigon, A., Jacob, D., Kang, H.-S., Raghavan,
1345 K., Lee, B., Lennard, C., Nikulin, G., O'Rourke, E., Rixen, M., Solman, S., Stephenson,
1346 T., and Tangang, F.: WCRP COordinated Regional Downscaling EXperiment (CORDEX):
1347 a diagnostic MIP for CMIP6, *Geosci. Model Dev.*, 9, 4087–4095,
1348 <https://doi.org/10.5194/gmd-9-4087-2016>, 2016

1349

1350 [Holtslag A, de Bruijn E, Pan HL \(1990\) A high resolution air mass transformation model](#)
1351 [for short-range weather fore-casting. Mon Weather Rev 118: 1561–1575](#)

1352

1353 [Hostetler SW, Bates GT, Giorgi F \(1993\) Interactive nesting of a lake thermal model within](#)
1354 [a regional climate model for climate change studies. J Geophys Res 98: 5045– 5057](#)

1355

1356 Huffman, G. J., and Coauthors, 2007: The TRMM Multisatellite Precipitation Analysis
1357 (TMPA): Quasi-global, multiyear, combined-sensor precipitation estimates at fine scales.
1358 *J. Hydrometeor.*, 8, 38–55, doi:<https://doi.org/10.1175/JHM560.1>

1359

1360 [Kiehl J, Hack J, Bonan G, Boville B, Breigleb B, Williamson D, Rasch P \(1996\)](#)
1361 [Description of the NCAR Commun -ity Climate Model \(CCM3\). National Center for](#)
1362 [Atmo spheric Research Tech Note NCAR/TN-420+ STR, NCAR, Boulder, CO](#)

1363

1364 Lean, H. W., P. A. Clark, M. Dixon, N. M. Roberts, A. Fitch, R. Forbes, and C. Halliwell,
1365 2008: Characteristics of high- resolution versions of the Met Office Unified Model for
1366 forecasting convection over the United Kingdom. *Mon. Wea. Rev.*, 136, 3408–3424,
1367 <https://doi.org/10.1175/2008MWR2332.1>.

1368

Deleted: <https://doi.org/10.1175/JHM560.1>

1370 Lind, P., D. Lindstedt, E. Kjellstrom, and C. Jones, 2016: Spatial and temporal
1371 characteristics of summer precipitation over central Europe in a suite of high-resolution
1372 climate models. *J. Climate*, 29, 3501–3518, <https://doi.org/10.1175/JCLI-D-15-0463.1>.

1373

1374 Hewitt, C. D., and J. A. Lowe, 2018: Toward a European climate prediction system. *Bull.*
1375 *Amer. Meteor. Soc.*, 99, 1997–2001, <https://doi.org/10.1175/BAMS-D-18-0022.1>.

1376 Hong, S.-Y., H.-M. H. Juang, and Q. Zhao, 1998: Implementation of prognostic cloud
1377 scheme for a regional spectral model, *Mon. Wea. Rev.*, 126, 2621–2639.

1378

1379 Hong, S.-Y., J. Dudhia, and S.-H. Chen, 2004: A Revised Approach to Ice Microphysical
1380 Processes for the Bulk Parameterization of Clouds and Precipitation, *Mon. Wea. Rev.*,
1381 132, 103–120.

1382

1383 Hong, S.-Y., and J.-O. J. Lim, 2006: The WRF Single-Moment 6-Class Microphysics
1384 Scheme (WSM6), *J. Korean Meteor. Soc.*, 42, 129–151

1385

1386 Hostetler SW, Bates GT, Giorgi F, 1993: Interactive Coupling of Lake Thermal Model with
1387 a Regional climate Model, *J. Geophys. Res.*, 98(D3), 5045-5057.

1388

1389 [Huffman, George J., David T. Bolvin, Eric J. Nelkin, David B. Wolff, Robert F. Adler, Guojun Gu, Yang Hong, Kenneth P. Bowman and Erich F. Stocker \(2007\). The TRMM Multisatellite Precipitation Analysis \(TMPA\): Quasi-Global, Multiyear, Combined-Sensor Precipitation Estimates at Fine Scales. DOI: 10.1175/JHM560.1.](#)

Formatted: Space Before: 12 pt, After: 12 pt

1393

1394 Joyce, Robert J., John E. Janowiak, Phillip A. Arkin, Pingping Xie, 2004: CMORPH: A
1395 Method that Produces Global Precipitation Estimates from Passive Microwave and
1396 Infrared Data at High Spatial and Temporal Resolution. *J. Hydrometeor*, 5, 487–503

1397

1398 Kain, J. S., 2004: The Kain–Fritsch convective parameterization: An update. *J. Appl.*
1399 *Meteor.*, 43, 170–181, [https://doi.org/10.1175/1520-0450\(2004\)043<0170:TKCPAU>2.0.CO;2](https://doi.org/10.1175/1520-0450(2004)043<0170:TKCPAU>2.0.CO;2).

Deleted: [https://doi.org/10.1175/1520-0450\(2004\)043<0170:TKCPAU>2.0.CO;2](https://doi.org/10.1175/1520-0450(2004)043<0170:TKCPAU>2.0.CO;2)

1401
1402 [Kain, J. S., and J. M. Fritsch, 1990: A one-dimensional entraining/ detraining plume model](#)
1403 [and its application in convective parameterization, *J. Atmos. Sci.*, 47, 2784–2802.](#)

1404
1405 Kendon, E. J., N. M. Roberts, C. A. Senior, and M. J. Roberts, 2012: Realism of rainfall
1406 in a very high-resolution regional climate model. *J. Climate*, 25, 5791–5806,
1407 <https://doi.org/10.1175/JCLI-D-11-00562.1>.

1408
1409 Kendon, E. J., and Coauthors, 2017: Do convection-permitting regional climate models
1410 improve projections of future precipitation change? *Bull. Amer. Meteor. Soc.*, 98, 79–93,
1411 <https://doi.org/10.1175/BAMS-D-15-0004.1>

1412
1413 Kessler, E., 1969: On the Distribution and Continuity of Water Substance in Atmospheric
1414 Circulations. *Meteor. Monogr.*, No. 32, Amer. Meteor. Soc., 84 pp.

1415
1416 Khairoutdinov, M. and Kogan, Y.: A new cloud physics parameterization in a large-eddy
1417 simulation model of marine stratocumulus, *B. Am. Meteorol. Soc.*, 128, 229–243, 2000

1418
1419 Klemp, J.B. and Dudhia, J.: An Upper Gravity-Wave Absorbing Layer for NWP
1420 Applications, *Monthly Weather Review*, 176, 3987–4004, 2008.

1421
1422 Klemp, J. B. and D. K. Lilly: Numerical simulation of hydrostatic mountain waves, *J.*
1423 *Atmos. Sci.*, 35, 78–107, 1978.

1424
1425 Lin, Y., Farley, R., and Orville, H.: Bulk parameterization of the snow field in a cloud
1426 model, *J. Appl. Meteor. Clim.*, 22, 1065–1092, 1983.

1427

1429 Marshall, J. S., and W. McK. Palmer, 1948: The distribution of raindrops with size. *J.*
1430 *Meteor.*, 5, 165–166.

1431

1432 [Matte, Dominic; Laprise, René; Thériault, Julie M.; Lucas-Picher, Philippe \(2017\). Spatial](#)
1433 [spin-up of fine scales in a regional climate model simulation driven by low-resolution](#)
1434 [boundary conditions. Climate Dynamics, 49\(1-2\), 563–574. doi:10.1007/s00382-016-](#)
1435 [3358-2](#)

1436

1437 [Mlawer, E. J., S. J. Taubman, P. D. Brown, M. J. Iacono, and S. A. Clough, 1997:](#)
1438 [Radiative transfer for inhomogeneous atmospheres: RRTM, a validated correlated-k](#)
1439 [model for the longwave. *J. Geophys. Res.*, 102, 16,663-16,682](#)

1440

1441 Nogherotto, R., Tompkins, A.M., Giuliani, G., Coppola, E. and Giorgi, F.: Numerical
1442 framework and performance of the new multiple-phase cloud microphysics scheme in
1443 RegCM4. 5: precipitation, cloud microphysics, and cloud radiative effects. *Geoscientific*
1444 *Model Development*, 9(7), 2533-2547, 2016

1445

1446 [Oleson, K. W., Lawrence, D. M., Bonan, G. B., Drewniak, B., Huang, M., Koven, C. D.,](#)
1447 [Levis, S., Li, F., Riley, W. J., Subin, Z. M., Swenson, S. C., Thornton, P. E., Bozbiyik, A.,](#)
1448 [Fisher, R., Kluzek, E., Lamarque, J. -F., Lawrence, P. J., Leung, L. R., Lipscomb, W.,](#)
1449 [Muszala, S., Ricciuto, D. M., Sacks, W., Sun, Y., Tang, J., and Yang, Z. -L:Technical](#)
1450 [Description of version 4.5 of the Community Land Model \(CLM\),Ncar Technical Note](#)
1451 [NCAR/TN-503+STR, National Center for Atmospheric Research, Boulder, CO, 422 pp.](#)
1452 [DOI: 10.5065/D6RR1W7M, 2013.](#)

1453

1454 [Pal JS, Small E, Eltahir E \(2000\) Simulation of regional-scale water and energy budgets:](#)
1455 [representation of subgrid cloud and precipitation processes within RegCM. *J Geo-phys*](#)
1456 [Res 105: 29579–29594](#)

1457

1458 Pal JS et al (2007) The ICTP RegCM3 and RegCNET: regional climate modeling for the
1459 developing world. *Bull Am Meteorol Soc* 88:1395–1409

1460

1461 Pichelli, E., Coppola, E., Sobolowski, S. *et al.* The first multi-model ensemble of regional
1462 climate simulations at kilometer-scale resolution part 2: historical and future simulations
1463 of precipitation. *Clim Dyn* (2021). <https://doi.org/10.1007/s00382-021-05657-4>

1464

1465 [Prein, Andreas F. and Andreas Gobiet \(2017\). 'Impacts of uncertainties in European](#)
1466 [gridded precipitation observations on regional climate analysis'. In: International Journal](#)
1467 [of Climatology. ISSN: 10970088. DOI: 10.1002/joc.4706](#)

1468

1469 Prein, A. F. *et al.* A review on regional convection-permitting climate modeling:
1470 demonstrations, prospects, and challenges. *Rev. Geophys.* 53, 323–361 (2015).

1471

1472 Ralph, F. M., P. J. Neiman, G. A. Wick, S. I. Gutman, M. D. Dettinger, D. R. Cayan, and A.
1473 B. White, 2006: Flooding on California's Russian River: Role of atmospheric rivers.
1474 *Geophys. Res. Lett.*, 33, L13801, <https://doi.org/10.1029/2006GL026689>

1475

1476 Ralph, F. M., M. D. Dettinger, M. M. Cairns, T. J. Galarneau, and J. Eylander, 2018:
1477 Defining “atmospheric river”: How the Glossary of Meteorology helped resolve a debate.
1478 *Bull. Amer. Meteor. Soc.*, 99, 837–839, <https://doi.org/10.1175/BAMS-D-17-0157.1>

1479

1480 Rutledge, S. A., and P. V. Hobbs, 1983: The mesoscale and microscale structure and
1481 organization of clouds and precipitation in midlatitude cyclones. Part VIII: A model for the
1482 “seeder-feeder” process in warm-frontal rainbands. *J. Atmos. Sci.*, 40, 1185–1206.

1483

1484 Skamarock WC, Klemp JB, Dudhia J, Gill DO, Barker DM, Duda MG, Huang XY, Wang
1485 W, Powers JG. 2008. ‘A description of the advanced research WRF version 3’, Technical
1486 Note NCAR/TN-475+STR. NCAR: Boulder, CO

1487

1488 Schwartz, C. S., 2014: Reproducing the September 2013 record- breaking rainfall over
1489 the Colorado Front Range with high- resolution WRF forecasts. *Wea. Forecasting*, 29,
1490 393–402, <https://doi.org/10.1175/WAF-D-13-00136.1>

1491
1492 Sitz, L. E., F. Sante, R. Farneti, R. Fuentes-Franco, E. Coppola, L. Mariotti, M. Reale, et
1493 al. 2017. "Description and Evaluation of the Earth System Regional Climate Model
1494 (RegCM-ES)." Journal of Advances in Modeling Earth Systems.
1495 doi:10.1002/2017MS000933
1496
1497 Song Y, Semazzi HMF, Xie L, Ogallo LJ, 2004: A coupled regional climate model for the
1498 Lake Victoria Basin of East Africa. *Int. J. Climatol.* 24: 57-75.
1499
1500 Sun X, Xie L, Semazzi F, Liu B, 2015: Effect of Lake Surface Temperature on the Spatial
1501 Distribution and Intensity of the Precipitation over the Lake Victoria Basin. *Mon. Wea.
Rev.* 143: 1179-1192.
1503
1504 Sundqvist, H., Berge, E., and Kristjansson, J.: Condensation and cloud parameterization
1505 studies with a mesoscale numerical weather prediction model, *Mon. Weather Rev.*, 117,
1506 1641–1657, 1989.
1507
1508 [Talling, J. F. \(1969\) The incidence of vertical mixing, and some biological and chemical
consequences, in tropical African lakes. Verh. Int. Ver. Limnol.](#) 17, 998-1012 DOI:
1509 [10.1080/03680770.1968.11895946](https://doi.org/10.1080/03680770.1968.11895946)
1511
1512 [Tiedtke, M., 1989, A comprehensive mass flux scheme for cumulus parametrization in
large-scale models. Mon. Weather Rev., 117, 1779–1800](#)
1514
1515 Tiedtke, M., 1993: Representation of Clouds in Large-Scale Models. *Mon. Wea. Rev.*,
1516 121, 3040–3061, [https://doi.org/10.1175/1520-0493\(1993\)121<3040:ROCILS>2.0.CO;2](https://doi.org/10.1175/1520-0493(1993)121<3040:ROCILS>2.0.CO;2)
1517
1518 Tiedtke, M., . 1996: An extension of cloud-radiation parameterization in the ECMWF
1519 model: The representation of subgrid-scale variations of optical depth. *Mon. Wea. Rev.*,
1520 124, 745–750
1521

Formatted: Line spacing: Multiple 1.15 li

Formatted: Font: (Default) Arial, 12 pt

1522 Tompkins, A.: Ice supersaturation in the ECMWF integrated fore-cast system, *Q. J. Roy.*
1523 *Meteor. Soc.*, 133, 53–63, 2007

1524

1525 Tripoli, G. J., and W. R. Cotton, 1980: A numerical investigation of several factors
1526 contributing to the observed variable intensity of deep convection over south Florida. *J.*
1527 *Appl. Meteor.*, 19, 1037–1063.

1528

1529 Williams PD. 2009. A proposed modification to the Robert–Asselin time filter. *Mon.*
1530 *Weather Rev.* 137: 2538–2546

1531

1532 Weisman, M. L., C. Davis, W. Wang, K. W. Manning, and J. B. Klemp, 2008: Experiences
1533 with 0–36-h explicit convective forecasts with the WRF-ARW model. *Wea. Forecasting*,
1534 23, 407–437, <https://doi.org/10.1175/2007WAF2007005.1>

1535

1536 Weusthoff, T., F. Ament, M. Arpagaus, and M. W. Rotach, 2010: Assessing the benefits
1537 of convection-permitting models by neighborhood verification: Examples from MAP D-
1538 PHASE. *Mon. Wea. Rev.*, 138, 3418–3433, <https://doi.org/10.1175/2010MWR3380.1>.

1539

1540 Zeng X, Zhao M, Dickinson RE (1998) Intercomparison of bulk aerodynamic algorithms
1541 for the computation of seasurface fluxes using TOGA COARE and TAO data. J Clim 11:
1542 2628–2644

1543

1544 Zhu, Y., and R. E. Newell, 1998: A proposed algorithm for moisture fluxes from
1545 atmospheric rivers. *Mon. Wea. Rev.*, 126, 725–735, [https://doi.org/10.1175/1520-0493\(1998\)126<0725:APAFMF>2.0.CO;2](https://doi.org/10.1175/1520-0493(1998)126<0725:APAFMF>2.0.CO;2).

1547

1548

Deleted: <https://doi.org/10.1175/2010MWR3380.1>

Page 2: [1] Deleted	Emanuela Pichelli	29/06/2021 14:02:00
▼		
Page 2: [1] Deleted	Emanuela Pichelli	29/06/2021 14:02:00
▼		
Page 2: [1] Deleted	Emanuela Pichelli	29/06/2021 14:02:00
▼		
Page 2: [1] Deleted	Emanuela Pichelli	29/06/2021 14:02:00
▼		
Page 2: [1] Deleted	Emanuela Pichelli	29/06/2021 14:02:00
▼		
Page 2: [1] Deleted	Emanuela Pichelli	29/06/2021 14:02:00
▼		
Page 2: [1] Deleted	Emanuela Pichelli	29/06/2021 14:02:00
▼		
Page 2: [1] Deleted	Emanuela Pichelli	29/06/2021 14:02:00
▼		
Page 2: [1] Deleted	Emanuela Pichelli	29/06/2021 14:02:00
▼		
Page 2: [1] Deleted	Emanuela Pichelli	29/06/2021 14:02:00
▼		
Page 2: [1] Deleted	Emanuela Pichelli	29/06/2021 14:02:00
▼		
Page 2: [2] Deleted	FILIPPO GIORGI	21/07/2021 07:20:00
▼		
Page 2: [2] Deleted	FILIPPO GIORGI	21/07/2021 07:20:00
▼		
Page 2: [2] Deleted	FILIPPO GIORGI	21/07/2021 07:20:00
▼		
Page 2: [2] Deleted	FILIPPO GIORGI	21/07/2021 07:20:00
▼		
Page 2: [3] Deleted	FILIPPO GIORGI	21/07/2021 07:39:00
▼		
Page 2: [3] Deleted	FILIPPO GIORGI	21/07/2021 07:39:00
▼		
Page 2: [3] Deleted	FILIPPO GIORGI	21/07/2021 07:39:00
▼		
Page 2: [3] Deleted	FILIPPO GIORGI	21/07/2021 07:39:00

Page 2: [3] Deleted	FILIPPO GIORGI	21/07/2021 07:39:00
Page 2: [3] Deleted	FILIPPO GIORGI	21/07/2021 07:39:00
Page 2: [3] Deleted	FILIPPO GIORGI	21/07/2021 07:39:00
Page 2: [4] Deleted	FILIPPO GIORGI	21/07/2021 08:10:00
Page 2: [4] Deleted	FILIPPO GIORGI	21/07/2021 08:10:00
Page 2: [4] Deleted	FILIPPO GIORGI	21/07/2021 08:10:00
Page 2: [4] Deleted	FILIPPO GIORGI	21/07/2021 08:10:00
Page 2: [4] Deleted	FILIPPO GIORGI	21/07/2021 08:10:00
Page 2: [4] Deleted	FILIPPO GIORGI	21/07/2021 08:10:00
Page 2: [4] Deleted	FILIPPO GIORGI	21/07/2021 08:10:00
Page 2: [4] Deleted	FILIPPO GIORGI	21/07/2021 08:10:00
Page 2: [4] Deleted	FILIPPO GIORGI	21/07/2021 08:10:00
Page 2: [4] Deleted	FILIPPO GIORGI	21/07/2021 08:10:00
Page 2: [4] Deleted	FILIPPO GIORGI	21/07/2021 08:10:00
Page 2: [4] Deleted	FILIPPO GIORGI	21/07/2021 08:10:00
Page 2: [5] Deleted	FILIPPO GIORGI	21/07/2021 07:47:00
Page 2: [5] Deleted	FILIPPO GIORGI	21/07/2021 07:47:00

Page 2: [5] Deleted	FILIPPO GIORGI	21/07/2021 07:47:00
▼		
Page 2: [6] Deleted	Emanuela Pichelli	29/06/2021 15:39:00
▼		
Page 2: [6] Deleted	Emanuela Pichelli	29/06/2021 15:39:00
▼		
Page 2: [7] Deleted	FILIPPO GIORGI	21/07/2021 07:48:00
▼		
Page 2: [7] Deleted	FILIPPO GIORGI	21/07/2021 07:48:00
▼		
Page 2: [7] Deleted	FILIPPO GIORGI	21/07/2021 07:48:00
▼		
Page 17: [8] Deleted	Paolo Stocchi	05/07/2021 11:11:00
▼		
Page 25: [9] Deleted	Paolo Stocchi	23/06/2021 12:47:00
▼		
Page 25: [10] Deleted	Emanuela Pichelli	13/07/2021 17:45:00
▼		
Page 30: [11] Deleted	Russell Glazer	24/06/2021 17:40:00
▼		
Page 34: [12] Deleted	Emanuela Pichelli	06/07/2021 16:04:00
▼		